PROCEEDINGS A

royalsocietypublishing.org/journal/rspa

Research

Cite this article: Erban R, Van Gorder RA. 2024 Langevin dynamics for a heavy particle immersed within a flow of light particles. *Proc. R. Soc. A* **480**: 20230851.
https://doi.org/10.1098/rspa.2023.0851

Received: 19 November 2023
Accepted: 23 August 2024

Subject Category:
Mathematics

Subject Areas:
applied mathematics, fluid mechanics, statistical physics

Keywords:
Brownian dynamics, micro-hydrodynamics, Langevin equation, Ornstein–Uhlenbeck process

Author for correspondence:
Radek Erban
e-mail: erban@maths.ox.ac.uk

Langevin dynamics for a heavy particle immersed within a flow of light particles

Radek Erban[1] and Robert A. Van Gorder[2]

[1]Mathematical Institute, University of Oxford, Radcliffe Observatory Quarter, Woodstock Road, Oxford OX2 6GG, UK
[2]Department of Mathematics and Statistics, University of Otago, P.O. Box 56, Dunedin 9054, New Zealand

RE, 0000-0001-8470-3763; RAVG, 0000-0002-8506-3961

A micro-hydrodynamics model based on elastic collisions of light point solvent particles with a heavy solute particle is investigated in the setting where the light particles have velocity distribution corresponding to a background flow. Considering a range of stationary background flows and distributions for the solvent particle velocities, the macroscopic Langevin-type description of the behaviour of the heavy particle is derived in the form of a generalized Ornstein–Uhlenbeck process. At leading order, the drift term in this process depends upon both the geometric structure of the background flow and the size of the heavy particle, while both drift and diffusion terms scale with moments of the light particle velocity distribution. Computational methods for simulating the micro-hydrodynamics model are then designed to confirm the theoretical results. To enable long-time calculations, simulations are performed in a frame co-moving with the heavy particle. Efficient methods for sampling the position and velocity distributions of incoming solvent particles at the boundaries of the co-moving frame are derived for a range of distributions of solvent particles. The simulations show good agreement with the theoretical results.

1. Introduction

The motion of a heavy particle within a heat bath of light particles serves as a canonical model for the molecular theory of Brownian motion [1–3]. In particular, collisions with light heat bath particles

THE ROYAL SOCIETY PUBLISHING

royalsocietypublishing.org/journal/rspa Proc. R. Soc. A 480: 20230851

result in momentum transfer to the heavy particle, thereby inducing Brownian motion of the heavy particle. The Brownian dynamics of the heavy particle can be modelled via a Langevin equation treating the contribution from random light particle collisions through drift and diffusion terms [4].

Consider the motion of a heavy solute particle (a ball with radius R and mass M) which is immersed within a solvent flow in domain $\Omega \subset \mathbb{R}^3$. The solvent is described as point particles that interact with the heavy solute particle when they collide with it. This configuration has been applied in a number of studies during the last 50 years, starting as one-dimensional [5] and three-dimensional [6] mechanical models of Brownian motion. We denote the position (centre) and velocity of the heavy solute particle by $\mathbf{X}$ and $\mathbf{V}$, respectively. We assume that all solvent particles have the same mass, denoted by m, and that they satisfy $m \ll M$. The positions and velocities of solvent particles are denoted by $\mathbf{x}_j$ and $\mathbf{v}_j$, respectively, where the particle index $j = 1,2,3, \ldots$ goes over all integers for theoretical studies [6,7] with spatial domain $\Omega = \mathbb{R}^3$. In contrast, there are a finite number of solvent particles in computational studies using finite-sized domains. To approximate the theoretical case of $\Omega = \mathbb{R}^3$ in computational studies, the solvent particles are introduced through suitable boundary conditions [8,9].

Denoting the dimensionless parameter $\mu = M/m$ and assuming that the collisions of the heavy particle with point solvent particles are without friction, the conservation of momentum and energy yield the following formulae for post-collision velocities [6,7]:

$$\tilde{\mathbf{V}} = [\mathbf{V}]^{\parallel} + \frac{\mu - 1}{\mu + 1}[\mathbf{V}]^{\perp} + \frac{2}{\mu + 1}[\mathbf{v}_j]^{\perp}, \tag{1.1}$$

$$\tilde{\mathbf{v}}_j = [\mathbf{v}_j]^{\parallel} + \frac{1}{\mu + 1}[\mathbf{v}_j]^{\perp} + \frac{2\mu}{\mu + 1}[\mathbf{V}]^{\perp}. \tag{1.2}$$

Here, $\mathbf{v}_j$ is the velocity of the solvent particle which collided with the heavy solute particle, tildes denote post-collision velocities, superscripts $\perp$ denote projections of velocities on the line through the centre of the solute particle and the collision point on its surface, and superscripts $\parallel$ denote tangential components. Micro-hydrodynamics models based on elastic collisions, equations (1.1) and (1.2), have been studied by a number of authors [5–10], all of whom investigate the macroscopic behaviour of the heavy particle for $\mu \gg 1$, where it provides a mechanical description of Brownian motion.

For example, consider the case of the infinite domain $\Omega = \mathbb{R}^3$ containing an infinite number of solvent particles with positions distributed according to a spatial Poisson process with constant density:

$$\lambda_\mu = \frac{3}{8R^2}\sqrt{\frac{(\mu + 1)\gamma}{2\pi D}}, \tag{1.3}$$

where D is a diffusion coefficient having dimension $[D] = [\text{length}]^2[\text{time}]^{-1}$ and γ is a friction coefficient having dimension $[\gamma] = [\text{time}]^{-1}$. Let the velocities of the solvent particles be distributed according to the Gaussian (Maxwell–Boltzmann) distribution

$$f_\mu(\mathbf{v}) = \frac{1}{\sigma_\mu^3(2\pi)^{3/2}}\exp\left[-\frac{v_1^2 + v_2^2 + v_3^2}{2\sigma_\mu^2}\right], \tag{1.4}$$

where $\mathbf{v} = (v_1, v_2, v_3)^{\mathrm{T}}$ and

$$\sigma_\mu = \sqrt{(\mu + 1)\,D\gamma}, \tag{1.5}$$

and assume that a solvent particle moves (between collisions) using the free flight, i.e. the position and velocity of the jth solvent particle satisfy

$$\frac{\mathrm{d}\mathbf{x}_j}{\mathrm{d}t} = \mathbf{v}_j \qquad \text{and} \qquad \frac{\mathrm{d}\mathbf{v}_j}{\mathrm{d}t} = \mathbf{0}, \tag{1.6}$$

between the elastic collisions governed by equations (1.1)–(1.2). Then, it can be shown [6,8] that, in the limit $\mu \to \infty$, the behaviour of the heavy particle converges (in the sense of distributions) to the Langevin dynamics given by

$$\mathrm{d}\mathbf{X} = \mathbf{V}\mathrm{d}t, \tag{1.7}$$

$$\mathrm{d}\mathbf{V} = -\gamma\mathbf{V}\,\mathrm{d}t + \gamma\sqrt{2D}\,\mathrm{d}\mathbf{W}, \tag{1.8}$$

where $\mathbf{W}$ is a three-dimensional vector of independent Wiener processes, and the drift term $-\gamma\mathbf{V}$ in equation (1.8) models friction.

Aside from standard Langevin dynamics of a heavy particle within a heat bath as governed by equations (1.7)–(1.8), there has been an interest in manipulating or controlling the motion of a heavy particle in a heat bath in some manner [11,12], with temperature gradients [13,14] and electromagnetic fields [15,16] used to bias the motion of the heavy particle. There is a history of literature extending the Brownian motion of a heavy object within a fluid flow comprising lighter particles [17–21]. In many of these studies, macroscale models are formulated for the heavy particle motion, informed by heat bath statistics of the type mentioned above. Often, the assumption that the size or mass of the light particles be much less than that of the heavy particle is necessary to make analytical progress; see [22,23]. Compare this with literature on the flow of heavy spheres within a given flow where the interaction of the sphere and the surrounding fluid is modelled at the macroscopic scale from the onset of the problem [24–27]. The Brownian motion of particles within certain flows has been suggested as a possible route to anomalous diffusion [28–30], motivating the development of more accurate models bridging microscale Brownian motion with macroscale flows [31]. The development of more accurate models of Brownian motion of a heavy particle immersed within generic flows aides us in better understanding the theory behind recent experimental results on the dynamics of Brownian particles within flows [32].

It is possible to reconcile models of Brownian motion of a heavy particle in a heat bath with macroscopic models of a heavy particle within a fluid flow by generalizing the heat bath to account for the directed motion of the heat bath particles according to a prescribed fluid flow. In some studies, a Langevin model for the motion of a heavy particle within a background flow has been asserted [33–38]. A derivation of Langevin dynamics for a heavy particle immersed in a non-zero background flow field taking the form of a linear shear flow was presented by Dobson *et al*. [39]. Earlier work described how to calibrate Gaussian particle distributions for the motion of a large particle within specific flows [40], highlighting the role shear flows have on particle diffusion at the macroscopic scale. Models allowing collisions of multiple particles within a heat bath are naturally more involved, and for a theoretical treatment of the problem, see [41], which obtains rigorous results for a continuous (repulsive) interaction potential between multiple heavy particles and heat bath particles, accounting for the possibility of multiple kinds of particle interactions. Kim and Karniadakis [42] study the difference in the Brownian motion of a heavy particle when the internal structure of interaction is considered versus the case when only elastic collisions are allowed. They also discuss differences between repulsive and attractive potentials.

In this paper, we extend the study of the Brownian motion of a heavy particle within a heat bath to account for general flows of the light particles, as well as for general forms of the light particle velocity distribution. We consider the problem where the heat bath particles correspond to a velocity distribution with mean value equal to a background vector field $\mathbf{u}$. The variance (and, higher moments) of these distributions account for sampling differences owing to the material of a flow. For instance, a rarefied gas will have a different distribution from a liquid which features more heat bath particle collisions. Indeed, the latter generalization is motivated by heavy-tailed velocity distributions that find application in high-energy granular

royalsocietypublishing.org/journal/rspa Proc. R. Soc. A 480: 20230851

gas experiments [43–46] and more generic composite velocity distributions that find application in the study of plasma flows [47,48], to give two examples. Momentum is transferred from the light heat bath particles to the heavy particle through collisions at the microscale, and we upscale this process to obtain the Langevin dynamics for the Brownian motion of the heavy particle at the mesoscale. The generic description accounts for a wide class of heat bath velocity distributions (each corresponding to specific physical scenarios) and mean flows. The generic, position-dependent distributions for the heat bath requires that the free-flight equations given by equation (1.6) have to be generalized to include the mean velocity dependence, as well. This is done in §2, where we introduce our microscopic model of the heat bath particles. We then derive the Langevin description for a heavy solute particle in §3. Our theoretical results take the form of a generalized Ornstein–Uhlenbeck process and are valid for generic forms of the velocity distribution of the solvent particles comprising the heat bath (which is of use even for heat bath configurations deviating from the standard Maxwell–Boltzmann statistics [49]), as well as for generic stationary mean flows. We then develop an efficient computational algorithm—in a frame co-moving with the heavy solute particle—to illustrate the theoretical results in §4. We discuss the key findings and possible future directions in §5.

2. Motion of the solvent particles

We assume that the mean motion of the heat bath is described by a vector field $\mathbf{u}(\mathbf{x})$ which is a stationary solution of a given fluid equation, such as the Navier–Stokes equations. Solvent particle velocities are then sampled according to a distribution

$$f_\mu(\mathbf{v},\mathbf{u}) = F_\mu(\mathbf{v}-\mathbf{u}), \tag{2.1}$$

where the function $F_\mu : \mathbb{R}^3 \to [0,\infty)$ satisfies the properties

$$\int_{\mathbb{R}^3} F_\mu(\mathbf{q})\,\mathrm{d}\mathbf{q} = 1 \qquad \text{and} \qquad \int_{\mathbb{R}^3} \|\mathbf{q}\|^4 F_\mu(\mathbf{q})\,\mathrm{d}\mathbf{q} < \infty, \tag{2.2}$$

for all $\mu \geq 0$. Note that equation (2.1) is a generalization of equation (1.4), which is covered by our framework for $\mathbf{u} \equiv \mathbf{0}$ and F_μ being the Gaussian distribution. In general, equation (2.1) states that the velocity distribution is centred around the vector field $\mathbf{u}$ and is therefore $\mathbf{u}$-dependent. Some important cases of the function $F_\mu : \mathbb{R}^3 \to [0,\infty)$ will be given in the product form

$$F_\mu(\mathbf{q}) = \frac{1}{\sigma_\mu^3}\mathcal{F}\left(\frac{q_1}{\sigma_\mu}\right)\mathcal{F}\left(\frac{q_2}{\sigma_\mu}\right)\mathcal{F}\left(\frac{q_3}{\sigma_\mu}\right), \tag{2.3}$$

where function $\mathcal{F} : \mathbb{R} \to [0,\infty)$ is given as the Gaussian, Laplace and generalized Gaussian distributions, respectively, see §3, but our initial derivation will consider F_μ in its full generality satisfying the conditions of equation (2.2).

Although the case where $\mathcal{F}$ is a Gaussian distribution is most common in the statistical physics literature, we note that the particular shape of a distribution is informed by the material comprising the heat bath particles, accounting for features such as the propensity for particle–particle interactions between the heat bath particles. Heavy-tailed distributions are shown to agree better with experiments on certain granular gases with high-energy particles [43–46]. Considering more detailed all-atom molecular dynamics models of solvent [50–52], non-Gaussian distributions of forces can be estimated from simulations and used to parameterize coarse-grained Brownian dynamics and Langevin dynamics models [53,54]. Rather than taking a prescribed functional form, F_μ can also be solved for separately from our analysis, and then inserted into our theory. For instance, to account for a background flow within which binary, ternary or higher-order collisions of light particles are important, one may solve the resulting Boltzmann equation for the light particle density [55]. However, to account for all

royalsocietypublishing.org/journal/rspa Proc. R. Soc. A 480: 20230851

possible distributions of relevance, we keep the form of F_μ general, requiring only that it satisfies equation (2.2).

We assume that the particle velocities are distributed according to distribution of equation (2.1) at any time $t \geq 0$ in our theoretical investigations. This assumption implies that the position and velocity of the jth solvent particle evolve according to the equations

$$\frac{\mathrm{d}\mathbf{x}_j}{\mathrm{d}t} = \mathbf{v}_j \qquad \text{and} \qquad \frac{\mathrm{d}\mathbf{v}_j}{\mathrm{d}t} = (\nabla \mathbf{u})\mathbf{v}_j \equiv \sum_{\ell=1}^{3} \frac{\partial \mathbf{u}}{\partial x_\ell} v_{j,\ell}, \tag{2.4}$$

where $\mathbf{v}_j = (v_{j,1}, v_{j,2}, v_{j,3})^{\mathrm{T}}$. This is a generalization of free-flight equation (1.6), which we obtain in the special case of zero flow $\mathbf{u}(\mathbf{x}) \equiv \mathbf{0}$ in equation (2.4).

In our illustrative simulations in §4, we initialize the velocities of particles according to equation (2.1) at time $t = 0$ and let their positions and velocities evolve according to equation (2.4). Assuming that the jth particle initial velocity is sampled as $\mathbf{v}_j^0$, its velocity at time t satisfies

$$\mathbf{v}_j(t) = \mathbf{u}(\mathbf{x}_j(t)) + \mathbf{v}_j^0.$$

This relation implies that the velocity distribution of equation (2.1) is preserved for all time $t > 0$ and we have (for $\Delta t > 0$)

$$\mathbf{v}_j(t+\Delta t) - \mathbf{v}_j(t) = \mathbf{u}\big(\mathbf{x}_j(t+\Delta t)\big) - \mathbf{u}(\mathbf{x}_j(t)) = \mathbf{u}\big(\mathbf{x}_j(t) + \mathbf{v}_j(t)\Delta t + \mathcal{O}(\Delta t)\big) - \mathbf{u}(\mathbf{x}_j(t)).$$

Applying the Taylor expansion, we get

$$\frac{\mathrm{d}\mathbf{v}_j}{\mathrm{d}t} = \lim_{\Delta t \to 0} \frac{\mathbf{v}_j(t+\Delta t) - \mathbf{v}_j(t)}{\Delta t} = \lim_{\Delta t \to 0} \big\{(\nabla \mathbf{u})\mathbf{v}_j(t) + \mathcal{O}(\Delta t)\big\} = (\nabla \mathbf{u})\mathbf{v}_j,$$

which is what was claimed in equation (2.4).

3. Derivation of Langevin dynamics

We assume that the generalization of the Langevin dynamics equations (1.7)–(1.8) for the motion of a heavy solute particle immersed within a heat bath comprising solvent particles moving with a prescribed flow profile $\mathbf{u}$ can be written as

$$\mathrm{d}\mathbf{X} = \mathbf{V}\,\mathrm{d}t, \tag{3.1}$$

$$\mathrm{d}\mathbf{V} = \boldsymbol{\alpha}(\mathbf{X}, \mathbf{V})\,\mathrm{d}t + \boldsymbol{\beta}(\mathbf{X}, \mathbf{V})\,\mathrm{d}\mathbf{W}, \tag{3.2}$$

where $\mathbf{W}$ is a three-dimensional vector of independent Wiener processes, and the drift and diffusion coefficients $\boldsymbol{\alpha}(\mathbf{X}, \mathbf{V})$ and $\boldsymbol{\beta}(\mathbf{X}, \mathbf{V})$ depend on the velocity field $\mathbf{u}(\mathbf{x})$ and the underlying distribution F_μ. The Langevin formulation (3.1)–(3.2) applies if the mass ratio of the Brownian particle to the solvent particles is large, i.e. for $m \ll M$, or equivalently for $\mu \gg 1$. To calculate the drift and diffusion coefficients, we first express them as integrals over the surface of the heavy particle:

$$\mathcal{S}(\mathbf{X}, R) \equiv \mathcal{S}(\mathbf{X}(t), R) = \big\{\mathbf{y} \in \mathbb{R}^3 \;\big|\; \|\mathbf{y} - \mathbf{X}(t)\| = R\big\}. \tag{3.3}$$

This is done, for general function F_μ satisfying the properties of equation (2.2), in the following theorem.

Theorem 3.1. *Let* $\mathbf{y}$ *be a point on the surface (3.3) of the heavy particle, i.e.,* $\mathbf{y} \in \mathcal{S}(\mathbf{X}, R)$*, and let vectors* $\boldsymbol{\eta}_2 \in \mathbb{R}^3$ *and* $\boldsymbol{\eta}_3 \in \mathbb{R}^3$ *be chosen so that* $\{(\mathbf{y} - \mathbf{X})/R, \boldsymbol{\eta}_2, \boldsymbol{\eta}_3\}$ *comprise an orthonormal basis for* $\mathbb{R}^3$*. Define the functions*:

royalsocietypublishing.org/journal/rspa Proc. R. Soc. A 480: 20230851

$$\psi_\ell(\mathbf{y}) = -\frac{2\lambda_\mu(y_\ell - X_\ell(t))}{(1+\mu)R}\int_0^\infty\int_{-\infty}^\infty\int_{-\infty}^\infty\left\{\xi_1 + \mathbf{V}(t)\cdot\left(\frac{\mathbf{y}-\mathbf{X}(t)}{R}\right)\right\}^2 \times F_\mu\left(-\left(\xi_1 + \mathbf{u}\cdot\frac{\mathbf{y}-\mathbf{X}(t)}{R}\right)\left(\frac{\mathbf{y}-\mathbf{X}(t)}{R}\right) + \sum_{i=2}^3(\xi_i - \mathbf{u}\cdot\boldsymbol{\eta}_i)\boldsymbol{\eta}_i\right)\mathrm{d}\xi_3\,\mathrm{d}\xi_2\,\mathrm{d}\xi_1 \tag{3.4}$$

and

$$\phi_{\ell,j}(\mathbf{y}) = \frac{4\lambda_\mu(y_\ell - X_\ell(t))(y_j - X_j(t))}{(1+\mu)^2R^2}\int_0^\infty\int_{-\infty}^\infty\int_{-\infty}^\infty\left\{\xi_1 + \mathbf{V}(t)\cdot\left(\frac{\mathbf{y}-\mathbf{X}(t)}{R}\right)\right\}^3 \times F_\mu\left(-\left(\xi_1 + \mathbf{u}\cdot\frac{\mathbf{y}-\mathbf{X}(t)}{R}\right)\left(\frac{\mathbf{y}-\mathbf{X}(t)}{R}\right) + \sum_{i=2}^3(\xi_i - \mathbf{u}\cdot\boldsymbol{\eta}_i)\boldsymbol{\eta}_i\right)\mathrm{d}\xi_3\,\mathrm{d}\xi_2\,\mathrm{d}\xi_1\,. \tag{3.5}$$

Then, the drift coefficient of the Itô stochastic differential equations (3.1)–(3.2) for the motion of the heavy solute particle can be expressed as the surface integral

$$\alpha_\ell(\mathbf{X},\mathbf{V}) = \int_{\mathcal{S}(\mathbf{X}(t),R)}\psi_\ell(\mathbf{y})\,\mathrm{d}A\,,\quad \ell = 1,2,3\,, \tag{3.6}$$

where $\mathrm{d}A$ *is the surface element centred at* $\mathbf{y}$*. The diffusion terms are given by the square root of the matrix having entries*

$$\beta^2_{\ell,j}(\mathbf{X},\mathbf{V}) = \int_{\mathcal{S}(\mathbf{X}(t),R)}\phi_{\ell,j}(\mathbf{y})\,\mathrm{d}A\,,\quad \ell,j = 1,2,3\,. \tag{3.7}$$

Proof. We assume, in the limit of large μ, that the velocity of the heavy particle evolves according to discretized SDE (3.2) which can be written as

$$V_\ell(t+\Delta t) = V_\ell(t) + \alpha_\ell(t)\Delta t + \beta_\ell(t)\sqrt{\Delta t}\,\chi_\ell\,, \tag{3.8}$$

where Δt is a (small) time-step and χ_ℓ, for $\ell = 1,2,3$, is a normally distributed random number with zero mean and unit variance. To determine $\boldsymbol{\alpha}$ and $\boldsymbol{\beta}$, we will match the mean and variance of the velocity jump in the microscopic solvent model to those of equation (3.8).

Let $\mathbf{y}\in\mathcal{S}(\mathbf{X},R)$ be a point on the surface of the heavy particle. We first find the distribution measuring the average change in velocity of the heavy particle owing to collisions near the surface point $\mathbf{y}$ during the time interval $[t, t+\Delta t]$; we will show that this quantity is to the leading order in Δt given as $\psi_\ell(\mathbf{y})\,\Delta t$, where $\psi_\ell(\mathbf{y})$ is expressed by equation (3.4). Then, $\psi_\ell(\mathbf{y})\,\Delta t\,\mathrm{d}A$ is the average change of the ℓth component of the velocity of the heavy molecule caused by collisions with heat bath particles in the time interval $[t, t+\Delta t]$ on the surface element $\mathrm{d}A$ centred at $\mathbf{y}$.

Consider a heat bath particle located at point $\mathbf{x}$ at time t which collides with the heavy particle at time $t+\tau\in(t, t+\Delta t)$ at the surface point which had position $\mathbf{y}$ at time t. Since Δt is small and the velocity jump of the heavy particle owing to collision with any one heat bath particle is small, we approximate $\mathbf{V}$ to be a constant in the interval $[t, t+\Delta t]$. That is to say, the change in $\mathbf{V}$ is $\mathcal{O}(\sqrt{\Delta t})$. At this level of approximation, the coordinate of the surface point at the collision time $t+\tau$ is equal to $\mathbf{y}+\tau\mathbf{V}$. Since the heat bath molecule moved from $\mathbf{x}$ to the collision point $\mathbf{y}+\tau\mathbf{V}$, its velocity before the collision was

$$\mathbf{v} = \frac{\mathbf{y}+\tau\mathbf{V}(t)-\mathbf{x}}{\tau} = \mathbf{V}(t) + \frac{\mathbf{y}-\mathbf{x}}{\tau}\,.$$

Making use of equation (1.1), we write the change in velocity of the heavy particle owing to the collision as

$$\widetilde{\mathbf{V}} - \mathbf{V} = \frac{2}{1+\mu}[\mathbf{v}-\mathbf{V}(t)]^\perp = \frac{2}{1+\mu}\left\{(\mathbf{v}-\mathbf{V}(t))\cdot\left(\frac{\mathbf{y}-\mathbf{X}(t)}{R}\right)\right\}\left(\frac{\mathbf{y}-\mathbf{X}(t)}{R}\right). \tag{3.9}$$

royalsocietypublishing.org/journal/rspa Proc. R. Soc. A 480: 20230851

The position $\mathbf{x}$ of the heat bath molecule must be in the half space above the plane tangent to the heavy particle at the collision point $\mathbf{y}+\tau\mathbf{V}(t)$; in particular, this means that the component of the velocity $\mathbf{v}$ in the direction $\mathbf{y}-\mathbf{X}(t)$ must be negative. We then parameterize the allowable velocities using

$$\mathbf{v} = -\xi_1\left(\frac{\mathbf{y}-\mathbf{X}(t)}{R}\right) + \xi_2\boldsymbol{\eta}_2 + \xi_3\boldsymbol{\eta}_3\,, \tag{3.10}$$

where $\xi_1 > 0$, $\xi_2, \xi_3 \in \mathbb{R}$, and $(\mathbf{y}-\mathbf{X}(t))/R, \boldsymbol{\eta}_2$ and $\boldsymbol{\eta}_3$ comprise an orthonormal basis for $\mathbb{R}^3$. Using this basis to represent velocity vectors, we rewrite equation (3.9) as

$$\widetilde{\mathbf{V}} - \mathbf{V} = -\frac{2}{(1+\mu)R}\left\{\xi_1 + \mathbf{V}(t)\cdot\left(\frac{\mathbf{y}-\mathbf{X}(t)}{R}\right)\right\}(\mathbf{y}-\mathbf{X}(t))\,. \tag{3.11}$$

For a given heat bath particle velocity $\mathbf{v}$, the set of possible starting points allowing for a collision with the heavy particle within the surface area element $\mathrm{d}A$ centred at $\mathbf{y}$ during the time interval $[t, t+\Delta t]$ is a cylinder of cross-sectional area $\mathrm{d}A$ and perpendicular height:

$$h = \Delta t(\mathbf{V}(t)-\mathbf{v})\cdot\left(\frac{\mathbf{y}-\mathbf{X}(t)}{R}\right) = \Delta t\left\{\xi_1 + \mathbf{V}(t)\cdot\left(\frac{\mathbf{y}-\mathbf{X}(t)}{R}\right)\right\}.$$

We assume the number of heat bath particles in this cylinder is Poisson distributed with mean λ_μ times its volume $h\,\mathrm{d}A$. The probability of collision of a heat bath particle with velocity in the interval $(\mathbf{v}, \mathbf{v}+\mathrm{d}\mathbf{v})$ with the surface element $\mathrm{d}A$ over the time interval $[t, t+\Delta t]$ reads

$$\lambda_\mu\Delta t\left\{\xi_1 + \mathbf{V}(t)\cdot\left(\frac{\mathbf{y}-\mathbf{X}(t)}{R}\right)\right\}\mathrm{d}A\, f_\mu\left(-\xi_1\left(\frac{\mathbf{y}-\mathbf{X}(t)}{R}\right) + \xi_2\boldsymbol{\eta}_2 + \xi_3\boldsymbol{\eta}_3\right)\mathrm{d}\mathbf{v}\,. \tag{3.12}$$

To find the average change in velocity of the heavy particle owing to collisions with $\mathrm{d}A$ during the time interval $[t, t+\Delta t]$, we multiply equation (3.11) by equation (3.12) and integrate over all possible velocities $\mathbf{v}$ parameterized by equation (3.10) obtaining

$$\begin{aligned}\psi_\ell(\mathbf{y})\,\Delta t\,\mathrm{d}A = &-\Delta t\,\mathrm{d}A\,\frac{2\lambda_\mu(y_\ell - X_\ell(t))}{(1+\mu)R}\int_0^\infty\int_{-\infty}^\infty\int_{-\infty}^\infty\left\{\xi_1 + \mathbf{V}(t)\cdot\left(\frac{\mathbf{y}-\mathbf{X}(t)}{R}\right)\right\}^2\\ &\times f_\mu\left(-\xi_1\left(\frac{\mathbf{y}-\mathbf{X}(t)}{R}\right) + \xi_2\boldsymbol{\eta}_2 + \xi_3\boldsymbol{\eta}_3\right)\mathrm{d}\xi_3\,\mathrm{d}\xi_2\,\mathrm{d}\xi_1\\ = &-\Delta t\,\mathrm{d}A\,\frac{2\lambda_\mu(y_\ell - X_\ell(t))}{(1+\mu)R}\int_0^\infty\int_{-\infty}^\infty\int_{-\infty}^\infty\left\{\xi_1 + \mathbf{V}(t)\cdot\left(\frac{\mathbf{y}-\mathbf{X}(t)}{R}\right)\right\}^2\\ &\times F_\mu\left(-\left(\xi_1 + \mathbf{u}\cdot\frac{\mathbf{y}-\mathbf{X}(t)}{R}\right)\left(\frac{\mathbf{y}-\mathbf{X}(t)}{R}\right) + \sum_{i=2}^3(\xi_i - \mathbf{u}\cdot\boldsymbol{\eta}_i)\boldsymbol{\eta}_i\right)\mathrm{d}\xi_3\,\mathrm{d}\xi_2\,\mathrm{d}\xi_1\,.\end{aligned}$$

Note that we have expressed $\mathbf{u}$ in terms of the basis vectors $\{(\mathbf{y}-\mathbf{X}(t))/R, \boldsymbol{\eta}_2, \boldsymbol{\eta}_3\}$, obtaining the representation

$$\mathbf{u} = \left\{\mathbf{u}\cdot\tfrac{\mathbf{y}-\mathbf{X}(t)}{R}\right\}\left(\tfrac{\mathbf{y}-\mathbf{X}(t)}{R}\right) + (\mathbf{u}\cdot\boldsymbol{\eta}_2)\boldsymbol{\eta}_2 + (\mathbf{u}\cdot\boldsymbol{\eta}_3)\boldsymbol{\eta}_3.$$

From here, we integrate this expression over the surface of the heavy molecule, and upon equating this integral to the average velocity jump in equation (3.8), we obtain equation (3.6) in the limit $\Delta t \to 0$.

To determine the diffusion term, we calculate the variance in the velocity jump in the ℓth direction from time t to time $t+\Delta t$ and equate this with $\beta_\ell^2(t)\Delta t$ in equation (3.8). It is also possible to have off-diagonal terms in the diffusion tensor, and we account for these as well. Since the mean velocity jump is $\mathcal{O}(\Delta t)$, the variance (to leading order) is the second moment of the velocity jump. We square the quantity (3.11), multiply it by equation (3.12), and then integrate over all possible parameterizations of $\mathbf{v}$ in equation (3.10), finding that the variance in

the ℓth component of the velocity jump of the heavy particle owing to collisions with $\mathrm{d}A$ over the time interval $[t, t+\Delta t]$ is $\phi_{\ell,j}(\mathbf{y})\,\Delta t\,\mathrm{d}A$, where

$$\begin{aligned}\phi_{\ell,j}(\mathbf{y}) &= \frac{4\lambda_\mu (y_\ell - X_\ell(t))(y_j - X_j(t))}{(1+\mu)^2 R^2}\int_0^\infty\int_{-\infty}^\infty\int_{-\infty}^\infty \left\{\xi_1 + \mathbf{V}(t)\cdot\left(\frac{\mathbf{y}-\mathbf{X}(t)}{R}\right)\right\}^3 \\ &\quad\times f_\mu\left(-\xi_1\left(\frac{\mathbf{y}-\mathbf{X}(t)}{R}\right) + \xi_2\boldsymbol{\eta}_2 + \xi_3\boldsymbol{\eta}_3\right)\mathrm{d}\xi_3\,\mathrm{d}\xi_2\,\mathrm{d}\xi_1 \\ &= \frac{4\lambda_\mu (y_\ell - X_\ell(t))(y_j - X_j(t))}{(1+\mu)^2 R^2}\int_0^\infty\int_{-\infty}^\infty\int_{-\infty}^\infty \left\{\xi_1 + \mathbf{V}(t)\cdot\left(\frac{\mathbf{y}-\mathbf{X}(t)}{R}\right)\right\}^3 \\ &\quad\times F_\mu\left(-\left(\xi_1 + \mathbf{u}\cdot\frac{\mathbf{y}-\mathbf{X}(t)}{R}\right)\left(\frac{\mathbf{y}-\mathbf{X}(t)}{R}\right) + \sum_{i=2}^3 (\xi_i - \mathbf{u}\cdot\boldsymbol{\eta}_i)\boldsymbol{\eta}_i\right)\mathrm{d}\xi_3\,\mathrm{d}\xi_2\,\mathrm{d}\xi_1\,.\end{aligned}$$

Integrating $\phi_{\ell,j}(\mathbf{y})\,\Delta t\,\mathrm{d}A$ over the surface $\mathcal{S}(\mathbf{X}(t), R)$ of the heavy molecule, and matching with second moment terms $\beta^2_{\ell,j}(t)\Delta t$ in equation (3.8), we obtain the 3×3 matrix $\boldsymbol{\beta}^2$ for which we then need to find the matrix root. However, since $\beta^2_{\ell,j}(t) = \beta^2_{j,\ell}(t)$ by symmetry of equation (3.5), the matrix $\boldsymbol{\beta}^2$ is real symmetric and hence such a root exists. ∎

Theorem 3.1 has given us a procedure by which to determine the drift and diffusion terms once a distribution F_μ is known. Importantly, we have needed to make no assumptions on the light particle distribution, other than require conditions (2.2) to hold, so our results are generic with respect to the distribution F_μ. Physical justification for the Langevin formulation (3.1)–(3.2) requires that the mass ratio be large, and we will exploit this to simplify the expressions in Theorem 3.1 in the $\mu \gg 1$ limit. This is equivalent to the large variance limit $\sigma_\mu \gg 1$. As we will see, this will still involve a rather generic class of distributions, holding physically relevant examples—such as the Gaussian distribution (1.4)—as special cases.

(a) Results for the large-mass-ratio limit

We simplify the results of Theorem 3.1 by accounting for the fact that the Langevin formulation (3.1)–(3.2) requires that the mass ratio be large, i.e. we assume $\mu \gg 1$. This is equivalent to $\sigma_\mu \gg 1$, and in this subsection, we derive functional forms for $\boldsymbol{\alpha}$ and $\boldsymbol{\beta}$ in this physically relevant limit. To make further progress along these lines, note that Theorem 3.1 has involved finding a triple integral over the moments of certain generic probability density functions. There is always one direction of integration along which a moment is contributed, and two which are effectively inert. We define the marginal density function

$$\widehat{f}_\mu(\xi_1) = \int_{-\infty}^\infty\int_{-\infty}^\infty f_\mu\left(-\xi_1\left(\frac{\mathbf{y}-\mathbf{X}(t)}{R}\right) + \xi_2\boldsymbol{\eta}_2 + \xi_3\boldsymbol{\eta}_3\right)\mathrm{d}\xi_3\,\mathrm{d}\xi_2\,, \tag{3.13}$$

where we have integrated over the two inert directions. Assuming that this integration can be carried out, let us assume the result takes the functional form

$$\widehat{f}_\mu(\xi) = \frac{1}{\sigma_\mu}\mathcal{F}\left(\frac{\xi}{\sigma_\mu}\right). \tag{3.14}$$

Here, $\mathcal{F}$ is still kept general, and is assumed to inherit properties of the density function F_μ in equation (2.2). We also assume the marginal density function (3.14) satisfies the moment relations

$$\int_a^\infty \xi^\kappa\,\widehat{f}_\mu(\xi)\,\mathrm{d}\xi \;=\; \mathcal{F}_\kappa\sigma_\mu^\kappa + \mathcal{O}\left(\frac{1}{\sigma_\mu}\right) \quad \text{as} \quad \sigma_\mu\to\infty, \quad \text{for} \quad \kappa = 0,1,2,3, \tag{3.15}$$

royalsocietypublishing.org/journal/rspa Proc. R. Soc. A 480: 20230851

where the leading term is independent of the specific finite value of a. The asymptotic relation (3.15) follows for many distributions from

$$\int_a^\infty \xi^\kappa \hat{f}_\mu(\xi)\,\mathrm{d}\xi = \int_a^\infty \xi^\kappa \frac{1}{\sigma_\mu}\mathcal{F}\left(\frac{\xi}{\sigma_\mu}\right)\mathrm{d}\xi = \sigma_\mu^\kappa \int_{a/\sigma_\mu}^\infty q^\kappa \mathcal{F}(q)\,\mathrm{d}q = \mathcal{F}_\kappa \sigma_\mu^\kappa - \sigma_\mu^\kappa \int_0^{a/\sigma_\mu} q^\kappa \mathcal{F}(q)\,\mathrm{d}q,$$

where

$$\mathcal{F}_\kappa = \int_0^\infty q^\kappa \mathcal{F}(q)\,\mathrm{d}q\,. \tag{3.16}$$

The leading-order terms in equation (3.15) are listed for a variety of specific distributions in table 1.

Theorem 3.2. *Assume that the marginal density function $\hat{f}_\mu(\xi_1)$ in equation (3.13) takes the form (3.14) and satisfies the asymptotic scalings (3.15). The Itô stochastic differential equations (3.1)–(3.2) for the motion of the heavy solute particle has drift and diffusion terms which take the form*

$$\boldsymbol{\alpha}(\mathbf{X},\mathbf{V}) = -\sqrt{2\pi}\,\mathcal{F}_1\gamma\left(\mathbf{V}-\mathbf{u}(\mathbf{X})-\boldsymbol{A}_R\left[\mathbf{u}(\mathbf{y})-\mathbf{u}(\mathbf{X})\right]\right) + \mathcal{O}\left(\frac{1}{\sigma_\mu}\right), \tag{3.17a}$$

and

$$\boldsymbol{\beta}(\mathbf{X},\mathbf{V}) = \sqrt{\sqrt{2\pi}\,\mathcal{F}_3 D}\,\gamma\,\mathbf{I} + \mathcal{O}\left(\frac{1}{\sigma_\mu}\right) \qquad \text{as} \quad \sigma_\mu \to \infty, \tag{3.17b}$$

where operator $\boldsymbol{A}_R$ given by

$$\boldsymbol{A}_R[\mathbf{w}] = \frac{3}{4\pi R^2}\int_{S(\mathbf{X}(t),R)} \frac{\mathbf{y}-\mathbf{X}(t)}{R}\left\{\mathbf{w}(\mathbf{y})\cdot\frac{\mathbf{y}-\mathbf{X}(t)}{R}\right\}\mathrm{d}A, \tag{3.18}$$

incorporates the geometry of the flow and finite-size effects of the heavy particle.

Proof. Using equation (3.13) in equation (3.4), we obtain

$$\psi_\ell(\mathbf{y}) = -\frac{2\lambda_\mu(y_\ell - X_\ell(t))}{(1+\mu)R}\int_0^\infty \left\{\xi_1 + \mathbf{V}(t)\cdot\left(\frac{\mathbf{y}-\mathbf{X}(t)}{R}\right)\right\}^2 \hat{f}_\mu\left(\xi_1 + \mathbf{u}\cdot\frac{\mathbf{y}-\mathbf{X}(t)}{R}\right)\mathrm{d}\xi_1\,.$$

Using equations (1.3) and (1.5), we get

$$\psi_\ell(\mathbf{y}) = -\frac{3\gamma(y_\ell - X_\ell(t))}{4\sigma_\mu R^3\sqrt{2\pi}}\int_{\mathbf{u}\cdot\frac{\mathbf{y}-\mathbf{X}(t)}{R}}^\infty \left\{\xi + (\mathbf{V}(t)-\mathbf{u})\cdot\left(\frac{\mathbf{y}-\mathbf{X}(t)}{R}\right)\right\}^2 \hat{f}_\mu(\xi)\,\mathrm{d}\xi\,.$$

Using equation (3.15), we obtain

$$\psi_\ell(\mathbf{y}) = -\frac{3\gamma}{4R^2\sqrt{2\pi}}\left(\frac{y_\ell - X_\ell(t)}{R}\right)\left(\mathcal{F}_2\sigma_\mu + 2\mathcal{F}_1(\mathbf{V}(t)-\mathbf{u})\cdot\left(\frac{\mathbf{y}-\mathbf{X}(t)}{R}\right) + \mathcal{O}\left(\frac{1}{\sigma_\mu}\right)\right),$$

as $\sigma_\mu \to \infty$. Substituting into equation (3.6) and using the following integration results on the surface of the sphere

$$\int_{S(\mathbf{X}(t),R)}\left(\frac{y_\ell - X_\ell(t)}{R}\right)\mathrm{d}\mathbf{y} = 0 \quad \text{for all} \quad \ell = 1,2,3\,, \quad \text{and}$$

$$\int_{S(\mathbf{X}(t),R)}\left(\frac{y_\ell - X_\ell(t)}{R}\right)\left(\frac{y_j - X_j(t)}{R}\right)\mathrm{d}\mathbf{y} = \frac{4\pi R^2}{3}\delta_{\ell,j} \quad \text{for all} \quad \ell, j = 1,2,3\,, \tag{3.19}$$

then, the drift term $\boldsymbol{\alpha}$ can be evaluated as

Table 1. Asymptotic scale constants in equation (3.15) for various marginal density functions $\mathcal{F}$, given by equation (3.16).

Distribution	$\mathcal{F}(q)$	$\mathcal{F}_0$	$\mathcal{F}_1$	$\mathcal{F}_2$	$\mathcal{F}_3$
Gaussian	$\frac{1}{\sqrt{2\pi}}\exp\left(-\frac{q^2}{2}\right)$	$\frac{1}{2}$	$\frac{1}{\sqrt{2\pi}}$	$\frac{1}{2}$	$\sqrt{\frac{2}{\pi}}$
Laplace	$\frac{1}{2\sqrt{2}}\exp\left(-\frac{\lvert q\rvert}{\sqrt{2}}\right)$	$\frac{1}{2}$	$\frac{1}{\sqrt{2}}$	2	$6\sqrt{2}$
Generalized Gaussian ($\theta = 3$ in equation (3.26))	$\frac{3}{2\sqrt{2}\,\Gamma(1/3)}\exp\left(-\left\lvert\frac{q}{\sqrt{2}}\right\rvert^3\right)$	$\frac{1}{2}$	$\frac{2^{-5/6}\Gamma(5/6)}{\sqrt{\pi}}$	$\frac{1}{\Gamma(1/3)}$	$\frac{\sqrt{2}}{3}$
Hyperbolic secant	$\frac{1}{2}\operatorname{sech}\left(\frac{\pi q}{2}\right)$	$\frac{1}{2}$	0.37122	$\frac{1}{2}$	0.97464
Uniform	$\begin{cases}\frac{1}{2} & \text{if} \quad \lvert q\rvert \le 1\\ 0 & \text{otherwise}\end{cases}$	$\frac{1}{2}$	$\frac{1}{4}$	$\frac{1}{6}$	$\frac{1}{8}$

$$\begin{aligned}\boldsymbol{\alpha}(\mathbf{X},\mathbf{V}) &= -\frac{3\mathcal{F}_1\gamma}{2R^2\sqrt{2\pi}}\int_{S(\mathbf{X}(t),R)}\left(\frac{\mathbf{y}-\mathbf{X}(t)}{R}\right)\left\{(\mathbf{V}(t)-\mathbf{u}(\mathbf{y}))\cdot\left(\frac{\mathbf{y}-\mathbf{X}(t)}{R}\right)\right\}\mathrm{d}\mathbf{y}+\mathcal{O}\left(\frac{1}{\sigma_\mu}\right)\\ &= -\frac{3\mathcal{F}_1\gamma}{2R^2\sqrt{2\pi}}\left[\int_{S(\mathbf{X}(t),R)}\left(\frac{\mathbf{y}-\mathbf{X}(t)}{R}\right)\left\{(\mathbf{V}(t)-\mathbf{u}(\mathbf{X}(t)))\cdot\left(\frac{\mathbf{y}-\mathbf{X}(t)}{R}\right)\right\}\mathrm{d}\mathbf{y}\right.\\ &\quad\left.-\int_{S(\mathbf{X}(t),R)}\left(\frac{\mathbf{y}-\mathbf{X}(t)}{R}\right)\left\{(\mathbf{u}(\mathbf{y})-\mathbf{u}(\mathbf{X}(t)))\cdot\left(\frac{\mathbf{y}-\mathbf{X}(t)}{R}\right)\right\}\mathrm{d}\mathbf{y}\right]+\mathcal{O}\left(\frac{1}{\sigma_\mu}\right),\end{aligned}$$

as $\sigma_\mu \to \infty$, which simplifies to equation (3.17a). Next, to simplify the diffusion terms, we use equations (3.13), (3.15), (1.3) and equation (1.5) in equation (3.5) to obtain

$$\begin{aligned}\phi_{\ell,j}(\mathbf{y}) &= \frac{4\lambda_\mu(y_\ell - X_\ell(t))(y_j - X_j(t))}{(1+\mu)^2R^2}\int_{\mathbf{u}\cdot\frac{\mathbf{y}-\mathbf{X}(t)}{R}}^{\infty}\left\{\xi+(\mathbf{V}(t)-\mathbf{u})\cdot\left(\frac{\mathbf{y}-\mathbf{X}(t)}{R}\right)\right\}^3\hat{f}_\mu(\xi)\,\mathrm{d}\xi\\ &= \frac{3D\gamma^2}{2R^2\sqrt{2\pi}}\frac{(y_\ell - X_\ell(t))(y_j - X_j(t))}{R^2}\left\{\mathcal{F}_3+\mathcal{O}\left(\frac{1}{\sigma_\mu}\right)\right\}.\end{aligned}$$

Substituting into equation (3.7) and using equation (3.19), we get

$$\begin{aligned}\beta^2_{\ell,j} &= \frac{3D\gamma^2}{2R^2\sqrt{2\pi}}\int_{S(\mathbf{X}(t),R)}\frac{(y_\ell - X_\ell(t))(y_j - X_j(t))}{R^2}\left\{\mathcal{F}_3+\mathcal{O}\left(\frac{1}{\sigma_\mu}\right)\right\}\mathrm{d}A\\ &= \sqrt{2\pi}\,\mathcal{F}_3 D\gamma^2\delta_{\ell,j}+\mathcal{O}\left(\frac{1}{\sigma_\mu}\right)\quad\text{for all}\quad \ell,j=1,2,3\,.\end{aligned}$$

As the squared diffusion tensor $\boldsymbol{\beta}^2$ is diagonal up to leading order, and since the full diffusion tensor $\boldsymbol{\beta}^2$ is real symmetric, we have that the square-root matrix exists and is diagonal up to leading order, resulting in equation (3.17b). ∎

Theorem 3.2 has allowed us to simplify the general integrals present in Theorem 3.1 by assuming a large mass ratio limit and then using the asymptotic property of equation (3.15) of the marginal distributions with finite-size effects encoded by operator $\mathbf{A}_R$. To further study finite mass ratio corrections, one could retain higher-order terms in powers of σ_μ^{-1}, developing a perturbation series for equation (3.17). To do so, one calculates higher-order terms in the asymptotic expansion of equation (3.15), finding

$$\int_a^\infty \xi^\kappa \hat{f}_\mu(\xi)\,\mathrm{d}\xi = \mathcal{F}_\kappa \sigma_\mu^\kappa - \frac{\mathcal{F}(0)\,a^{\kappa+1}}{(\kappa+1)\,\sigma_\mu} - \frac{\mathcal{F}'(0)\,a^{\kappa+2}}{(\kappa+2)\,\sigma_\mu^2} + \mathcal{O}\left(\frac{1}{\sigma_\mu^3}\right) \quad \text{for } \kappa = 0, 1, 2, 3\,. \tag{3.20}$$

When the velocity distribution of light particles is symmetric about the velocity field, $\mathcal{F}'(0) = 0$, and hence the $\mathcal{O}(\sigma_\mu^{-2})$ terms drop out. One then uses these terms in the integrals for $\psi_\ell(\mathbf{y})$ and $\phi_{\ell,j}(\mathbf{y})$, adding additional terms to the integrals evaluated in the proof of Theorem 3.2. We illustrate the asymptotic expansion of equation (3.20) with the following example.

Example 3.1. Consider the Gaussian distribution with mean zero and variance σ_μ. We calculate

$$\begin{aligned}
\int_a^\infty \hat{f}_\mu(\xi)\,\mathrm{d}\xi &= \frac{1}{2}\left[1 - \operatorname{erf}\left(\frac{a}{\sqrt{2}\,\sigma_\mu}\right)\right] = \mathcal{F}_0 - \frac{a}{\sqrt{2\pi}\,\sigma_\mu} + \mathcal{O}\left(\frac{1}{\sigma_\mu^3}\right),\\
\int_a^\infty \xi\,\hat{f}_\mu(\xi)\,\mathrm{d}\xi &= \frac{\sigma_\mu}{\sqrt{2\pi}} \exp\left(-\frac{a^2}{2\sigma_\mu^2}\right) = \mathcal{F}_1\,\sigma_\mu - \frac{a^2}{2\sqrt{2\pi}\,\sigma_\mu} + \mathcal{O}\left(\frac{1}{\sigma_\mu^3}\right),\\
\int_a^\infty \xi^2\,\hat{f}_\mu(\xi)\,\mathrm{d}\xi &= \frac{\sigma_\mu}{2\sqrt{\pi}}\left[\sqrt{\pi}\,\sigma_\mu\left\{1 - \operatorname{erf}\left(\frac{a}{\sqrt{2}\sigma_\mu}\right)\right\} + \sqrt{2}\,a \exp\left(-\frac{a^2}{2\sigma_\mu^2}\right)\right]\\
&= \mathcal{F}_2\,\sigma_\mu^2 - \frac{a^3}{3\sqrt{2\pi}\,\sigma_\mu} + \mathcal{O}\left(\frac{1}{\sigma_\mu^3}\right),\\
\int_a^\infty \xi^3\,\hat{f}_\mu(\xi)\,\mathrm{d}\xi &= \frac{\sigma_\mu}{\sqrt{2\pi}}\left(2\sigma_\mu^2 + a^2\right) \exp\left(-\frac{a^2}{2\sigma_\mu^2}\right) = \mathcal{F}_3\,\sigma_\mu^3 - \frac{a^4}{4\sqrt{2\pi}\,\sigma_\mu} + \mathcal{O}\left(\frac{1}{\sigma_\mu^3}\right).
\end{aligned}$$

For instance, when the mass ratio $\mu = M/m$ is equal to 10^4, the first finite-size correction is $\mathcal{O}(\sigma_\mu^{-1}) = \mathcal{O}(10^{-2})$ while the error term is of size $\mathcal{O}(\sigma_\mu^{-3}) = \mathcal{O}(10^{-6})$. As such, the leading-order terms in Theorem 3.2 will be sufficient for cases with mass ratios of these sizes.

(b) Role of velocity distribution shape on the drift and diffusion

To better understand Theorem 3.2, it is worth considering how the shape of the light particle velocity distribution influences the drift and diffusion terms.

Corollary 3.1. *If the light particles are distributed according to Maxwell–Boltzmann statistics (equation (1.4)), then $\mathcal{F}$ is Gaussian, $\mathcal{F}_1 = 1/\sqrt{2\pi}$, $\mathcal{F}_3 = \sqrt{2/\pi}$ and equation (3.17) reduce to*

$$\boldsymbol{\alpha}(\mathbf{X}, \mathbf{V}) = -\gamma\{\mathbf{V} - \mathbf{u}(\mathbf{X}) - \boldsymbol{A}[\mathbf{u}(\mathbf{y}) - \mathbf{u}(\mathbf{X})]\} + \mathcal{O}\left(\frac{1}{\sigma_\mu}\right), \tag{3.21a}$$

$$\boldsymbol{\beta}(\mathbf{X}, \mathbf{V}) = \sqrt{2D\gamma}\,\mathbf{I} + \mathcal{O}\left(\frac{1}{\sigma_\mu}\right), \qquad \text{as} \quad \sigma_\mu \to \infty\,. \tag{3.21b}$$

Corollary 3.1 shows that Theorem 3.2 reduces to the result (1.8) for the special case $\mathbf{u} \equiv \mathbf{0}$. Next, we consider more general velocity distributions $F_\mu(\mathbf{q})$ with thin or heavy tails. For any fixed shape parameter $\theta > 0$, a generalized Gaussian distribution takes the form

$$F_\mu(\mathbf{q}; \theta) = \left(\frac{\theta}{2\sqrt{2}\,\Gamma(1/\theta)\,\sigma_\mu}\right)^3 \exp\left(-\left(\frac{\|\mathbf{q}\|}{\sqrt{2}\,\sigma_\mu}\right)^\theta\right). \tag{3.22}$$

This may seem like a distribution that will not separate into the product form of equation (2.3) for general θ, making the calculation of a marginal distribution complicated or even impossible. However, this all depends upon how we define the vector norm $\|\,\mathbf{q}\,\|$. Let us take

$$\|\,\mathbf{q}\,\| = \|\,\mathbf{q}\,\|_\theta := \left(\sum_{\ell=1}^{3} |\,q_\ell\,|^\theta\right)^{1/\theta}.$$

royalsocietypublishing.org/journal/rspa Proc. R. Soc. A 480: 20230851

Then, equation (3.22) becomes

$$F_\mu(\mathbf{q};\theta) = \prod_{\ell=1}^{3} \frac{\theta}{2\sqrt{2}\,\Gamma(1/\theta)\,\sigma_\mu} \exp\left(-\left(\frac{|q_\ell|}{\sqrt{2}\,\sigma_\mu}\right)^\theta\right). \tag{3.23}$$

Although the $\theta = 2$ (Maxwellian) distribution is most common in the statistical physics literature, we remark that other values of θ have applications. The particular shape of a distribution is informed by the physics of the light particles, accounting for features such as the propensity for particle–particle interactions between the heat bath particles. Heavy-tailed distributions with $\theta = 1$ (Laplace) [46] and $\theta = 3/2$ [43–45] are arguably better distributions for certain granular gases in experiments with high-energy particles. Non-Gaussian distributions of forces can also be estimated from more detailed all-atom molecular dynamics models of solvent [50–54].

Theorem 3.3. *Let the distribution of solvent particle velocities follow a generalized Gaussian distribution of the form of equation (3.22) with vector norm* $\|\mathbf{q}\| = \|\mathbf{q}\|_\theta$, *then drift and diffusion terms in equation (3.17a) and (3.17b) reduce to*

$$\boldsymbol{\alpha}(\mathbf{X},\mathbf{V}) = -\chi_1(\theta)\,\gamma\{\mathbf{V} - \mathbf{u}(\mathbf{X}) - \boldsymbol{A}[\mathbf{u}(\mathbf{y}) - \mathbf{u}(\mathbf{X})]\} + \mathcal{O}\left(\frac{1}{\sigma_\mu}\right), \tag{3.24a}$$

$$\boldsymbol{\beta}(\mathbf{X},\mathbf{V}) = \chi_2(\theta)\sqrt{2D}\,\gamma\,\mathbf{I} + \mathcal{O}\left(\frac{1}{\sigma_\mu}\right), \tag{3.24b}$$

as $\sigma_\mu \to \infty$, *where the scale factors read*

$$\chi_1(\theta) = 2^{(2-\theta)/\theta}\,\Gamma\left(\frac{2+\theta}{2\theta}\right) \quad \text{and} \quad \chi_2(\theta) = \frac{8^{1/\theta}}{2\pi^{1/4}}\sqrt{\Gamma\left(\frac{2+\theta}{2\theta}\right)\Gamma\left(\frac{4+\theta}{2\theta}\right)}. \tag{3.25}$$

Here, Γ *denotes the gamma function, and the scale factors are well-defined for all* $\theta > 0$.

Proof. Using equation (3.23) we can integrate over the two inert coordinates in equation (3.13), constructing the marginal distribution function according to equation (3.14),

$$\mathcal{F}(q) = \frac{\theta}{2\sqrt{2}\,\Gamma(1/\theta)} \exp\left(-\left(\frac{|q|}{\sqrt{2}}\right)^\theta\right), \tag{3.26}$$

with $\theta > 0$. Using equation (3.16), we have

$$\mathcal{F}_1 = \frac{2^{(4-3\theta)/(2\theta)}}{\sqrt{\pi}}\,\Gamma\left(\frac{2+\theta}{2\theta}\right) \quad \text{and} \quad \mathcal{F}_3 = \frac{8^{(4-\theta)/(2\theta)}}{\pi}\,\Gamma\left(\frac{2+\theta}{2\theta}\right)\Gamma\left(\frac{4+\theta}{2\theta}\right).$$

The result then follows from an application of Theorem 3.2. ∎

We have that both scale factors of equations (3.25) are decreasing functions of θ, with

$$\lim_{\theta\to 0^+} \chi_{1,2}(\theta) = \infty, \quad \lim_{\theta\to\infty} \chi_1(\theta) = \frac{\sqrt{\pi}}{2} \approx 0.88623, \quad \text{and} \quad \lim_{\theta\to\infty} \chi_2(\theta) = \frac{\pi^{1/4}}{2} \approx 0.66567.$$

Therefore, when $0 < \theta < 2$, the heavy tails result in a sampling of a greater proportion of larger velocities, resulting in both faster drift and larger diffusion when compared with the Gaussian (Maxwell–Boltzmann) results. When $\theta > 2$, the thin tails result in sampling of a greater proportion of smaller velocities, resulting in both slower drift and smaller diffusion when compared with the Gaussian results. We list key values of these scale factors in table 2, while also providing a plot of each as a function of θ. We conclude this section with an example where Theorem 3.2 is not applicable, necessitating the more general treatment of Theorem 3.1.

Example 3.2. Assume that the solvent particle velocities are sampled according to the Dirac delta distribution $f_\mu(\mathbf{v},\mathbf{u}) = F_\mu(\mathbf{v}-\mathbf{u})$, where $F_\mu(\mathbf{q})$ is in the product form of equation (2.3) for $\mathcal{F}(q) = \delta(q)$. Then, we have

Table 2. Constants scaling the drift and diffusion terms of equation (3.24) in Theorem 3.3 for various marginal density functions $\mathcal{F}$ according to equation (3.25) (left) and plots of the scale factors $\chi_1(\theta)$ and $\chi_2(\theta)$ (right).

Distribution	θ	$\chi_1(\theta)$	$\chi_2(\theta)$
Heavy-tail limit	$\theta \to 0^+$	∞	∞
Laplace	$\theta = 1$	1.77245	3.26109
Heavy-tailed Gaussian	$\theta = 3/2$	1.16885	1.40335
Maxwell–Boltzmann	$\theta = 2$	1	1
Thin-tailed Gaussian	$\theta = 3$	0.89592	0.76865
Thin-tail limit	$\theta \to \infty$	0.88623	0.66567

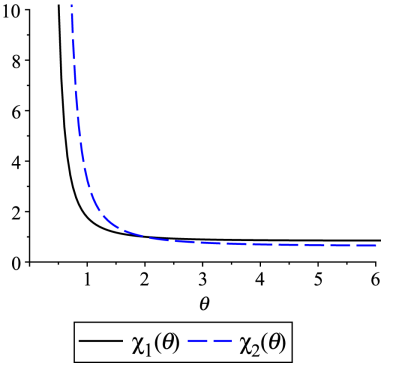

$$\int_a^\infty \xi^\kappa \hat{f}_\mu(\xi)\,\mathrm{d}\xi = \int_a^\infty \xi^\kappa \frac{1}{\sigma_\mu}\delta\!\left(\frac{\xi}{\sigma_\mu}\right)\mathrm{d}\xi = \begin{cases} 1 - H(a) & \text{if } \kappa = 0, \\ 0 & \text{if } \kappa = 1,2,3, \end{cases}$$

where $H(\cdot)$ is the Heaviside step function, so the marginal distribution depends on a and yet not on σ_μ. Define $\mathcal{S}_-(\mathbf{X}(t), R) \subset \mathcal{S}(\mathbf{X}(t), R)$ to be the set

$$\mathcal{S}_-(\mathbf{X}(t), R) = \left\{ \mathbf{y} \in \mathcal{S}(\mathbf{X}(t), R) \quad \text{and} \quad \mathbf{u}(\mathbf{y}) \cdot \left(\frac{\mathbf{y} - \mathbf{X}}{R}\right) < 0 \right\}.$$

Applying Theorem 3.1, the drift coefficient of the Itô stochastic differential equations (3.1)–(3.2) for the motion of the heavy solute particle can be expressed as the surface integral

$$\alpha_\ell(\mathbf{X}, \mathbf{V}) = -\frac{2\lambda_\mu}{1+\mu}\int_{\mathcal{S}_-(\mathbf{X}(t),R)} \left(\frac{y_\ell - X_\ell(t)}{R}\right)\left\{(\mathbf{V}(t) - \mathbf{u}) \cdot \left(\frac{\mathbf{y} - \mathbf{X}(t)}{R}\right)\right\}^2 \mathrm{d}A, \quad \ell = 1,2,3,$$

where $\mathrm{d}A$ is the surface element centred at $\mathbf{y}$. Also, Theorem 3.1 implies that the diffusion terms are given by the square root of the matrix having entries

$$\beta^2_{\ell,j}(\mathbf{X}, \mathbf{V}) = \frac{4\lambda_\mu}{(1+\mu)^2}\int_{\mathcal{S}_-(\mathbf{X}(t),R)} \left(\frac{y_\ell - X_\ell(t)}{R}\right)\left(\frac{y_j - X_j(t)}{R}\right)\left\{(\mathbf{V}(t) - \mathbf{u}) \cdot \left(\frac{\mathbf{y} - \mathbf{X}(t)}{R}\right)\right\}^3 \mathrm{d}A,$$

for each pair $\ell, j = 1,2,3$. Since the integral is performed over $\mathcal{S}_-$ rather than $\mathcal{S}$ this builds an asymmetry into the dynamics, where the structure of this asymmetry strongly depends upon the geometry of the flow $\mathbf{u}(\mathbf{y})$ local to the heavy particle.

As previously discussed in §2, the choice of probability density for the light particle velocities serves as a model for the specific material comprising the heat bath. Probability densities viewed as a sum of simpler densities find application in the statistical understanding of certain plasma flows [47,48], where they allow for better agreement with experimental observations than would single simple distributions. As such, it is worth extending our results to this case. We consider a distribution function for the velocities of the light particles given by

$$f_\mu(\mathbf{v}, \mathbf{u}) = F_\mu(\mathbf{v} - \mathbf{u}) \quad \text{where} \quad F_\mu(\mathbf{q}) = \sum_{\ell=1}^{\ell^*} c_\ell F_{\mu,\ell}(\mathbf{q}) \tag{3.27}$$

royalsocietypublishing.org/journal/rspa Proc. R. Soc. A 480: 20230851

and each function $F_{\mu,\ell}$ obeys the properties (2.2) while the coefficients are subject to the constraint $\sum_{\ell=1}^{\ell^*} c_\ell = 1$, so that in turn $F_\mu(\mathbf{q})$ also obeys the properties of equation (2.2). We assume that each $F_{\mu,\ell}$ has corresponding marginal distribution function $\widehat{F}_{\mu,\ell}(\xi) = \sigma_\mu^{-1}\widetilde{\mathcal{F}}_\ell(\xi/\sigma_\mu)$ satisfying the asymptotic scaling

$$\int_a^\infty \xi^\kappa \frac{1}{\sigma_\mu}\widetilde{\mathcal{F}}_\ell\left(\frac{\xi}{\sigma_\mu}\right)\mathrm{d}\xi = \mathcal{F}_{\ell;\kappa}\sigma_\mu^\kappa + \mathcal{O}\left(\frac{1}{\sigma_\mu}\right) \tag{3.28}$$

as $\sigma_\mu \to \infty$, given $\kappa = 0,1,2,3,\ldots$, where the leading term is independent of the value of a.

Theorem 3.4. *Let the marginal distribution of light particle velocities takes the form of a superposition of simpler densities (3.27). Then, the drift and diffusion terms in equation (3.17) reduce to*

$$\boldsymbol{\alpha}(\mathbf{X},\mathbf{V}) = -\sqrt{2\pi}\left(\sum_{\ell=1}^{\ell^*}\mathcal{F}_{\ell;1}\right)\gamma\{\mathbf{V}-\mathbf{u}(\mathbf{X})-\boldsymbol{A}[\mathbf{u}(\mathbf{y})-\mathbf{u}(\mathbf{X})]\} + \mathcal{O}\left(\frac{1}{\sigma_\mu}\right), \tag{3.29a}$$

$$\boldsymbol{\beta}(\mathbf{X},\mathbf{V}) = \sqrt{\sqrt{\frac{\pi}{2}}\sum_{\ell=1}^{\ell^*}\mathcal{F}_{\ell;3}}\sqrt{2D}\,\gamma\,\mathbf{I} + \mathcal{O}\left(\frac{1}{\sigma_\mu}\right) \quad \text{as} \quad \sigma_\mu \to \infty\,. \tag{3.29b}$$

Proof. Using equation (3.27), we can integrate over the two inert coordinates in equation (3.13), constructing the marginal distribution function according to equation (3.14), in the form $\mathcal{F}(q) = \sum_{\ell=1}^{\ell^*} c_\ell \widetilde{\mathcal{F}}_\ell(q)$. From here, we calculate the asymptotic scalings needed to describe the drift and diffusion terms, $\mathcal{F}_1 = \sum_{\ell=1}^{\ell^*}\mathcal{F}_{\ell;1}$ and $\mathcal{F}_3 = \sum_{\ell=1}^{\ell^*}\mathcal{F}_{\ell;3}$. The result then follows from an application of Theorem 3.2. ∎

Example 3.3. Consider a generalized Gaussian distribution for the light particle velocities with polynomial factors that influence the shape of the distribution (for applications of such distributions in plasma physics, see [47,48,56]), say equation (3.27) with each $F_{\mu,\ell}(\mathbf{q})$ chosen so that the marginal distribution $\mathcal{F}(q)$ takes the form

$$\mathcal{F}(q) = \sum_{\ell=1}^{\ell^*} c_\ell \frac{q^{2\ell}\exp(-q^2/2)}{2^{\ell+\frac{1}{2}}\Gamma\left(\ell+\frac{1}{2}\right)}, \tag{3.30}$$

with the coefficients satisfying $\sum_{\ell=0}^{\ell^*} c_\ell = 1$. We find for equation (3.30) that the leading-order terms in the moments (3.15) take the form

$$\mathcal{F}_0 = \frac{1}{2}, \quad \mathcal{F}_1 = \sum_{\ell=1}^{\ell^*}\frac{c_\ell\Gamma(\ell+1)}{\sqrt{2}\,\Gamma\left(\ell+\frac{1}{2}\right)}, \quad \mathcal{F}_2 = \sum_{\ell=1}^{\ell^*}\frac{c_\ell\Gamma\left(\ell+\frac{3}{2}\right)}{\Gamma\left(\ell+\frac{1}{2}\right)}, \quad \mathcal{F}_3 = \sum_{\ell=1}^{\ell^*}\frac{\sqrt{2}\,c_\ell\Gamma(\ell+2)}{\Gamma\left(\ell+\frac{1}{2}\right)}\,. \tag{3.31}$$

Applying Theorem 3.4, the drift and diffusion terms in equation (3.17) reduce to

$$\boldsymbol{\alpha}(\mathbf{X},\mathbf{V}) = -\sqrt{\pi}\left(\sum_{\ell=1}^{\ell^*}\frac{c_\ell\Gamma(\ell+1)}{\Gamma\left(\ell+\frac{1}{2}\right)}\right)\gamma\{\mathbf{V}-\mathbf{u}(\mathbf{X})-\boldsymbol{A}[\mathbf{u}(\mathbf{y})-\mathbf{u}(\mathbf{X})]\} + \mathcal{O}\left(\frac{1}{\sigma_\mu}\right), \tag{3.32a}$$

$$\boldsymbol{\beta}(\mathbf{X},\mathbf{V}) = \sqrt{\sqrt{\pi}\sum_{\ell=1}^{\ell^*}\frac{c_\ell\Gamma(\ell+2)}{\Gamma\left(\ell+\frac{1}{2}\right)}}\sqrt{2D}\,\gamma\,\mathbf{I} + \mathcal{O}\left(\frac{1}{\sigma_\mu}\right) \quad \text{as} \quad \sigma_\mu \to \infty\,. \tag{3.32b}$$

(c) Finite-size effects and the role of the flow geometry

While our results are valid for generic vector fields $\mathbf{u}$ modelling the mean flow, it is worth considering some specific examples to illustrate the theory. In this subsection, we consider how the drift term (3.17a) in Theorem 3.2 behaves under specific stationary flows $\mathbf{u}$ of a given geometric structure. We first derive a general result for flows which are smooth enough. It is given as Theorem 3.5, which is then applied to several specific choices of flows in the corollaries. Theorem 3.5 can be applied to a number of flows commonly used in the fluid mechanics literature; see [57] and [58] for many examples and additional motivation behind some of the flows we study in this subsection.

Theorem 3.5. *Let* $\mathbf{u} \in C^2(\mathbb{R}^3)$. *Then, the finite-size correction (3.18) in the drag term (3.17a) reads*

$$\boldsymbol{A}[\mathbf{u}(\mathbf{y}) - \mathbf{u}(\mathbf{X})] = \frac{R^2}{10}\begin{pmatrix} 3\frac{\partial^2 u_1}{\partial y_1^2} + \frac{\partial^2 u_1}{\partial y_2^2} + \frac{\partial^2 u_1}{\partial y_3^2} + 2\frac{\partial^2 u_2}{\partial y_1 \partial y_2} + 2\frac{\partial^2 u_3}{\partial y_1 \partial y_3} \\ \frac{\partial^2 u_2}{\partial y_1^2} + 3\frac{\partial^2 u_2}{\partial y_2^2} + \frac{\partial^2 u_2}{\partial y_3^2} + 2\frac{\partial^2 u_1}{\partial y_1 \partial y_2} + 2\frac{\partial^2 u_3}{\partial y_2 \partial y_3} \\ \frac{\partial^2 u_3}{\partial y_1^2} + \frac{\partial^2 u_3}{\partial y_2^2} + 3\frac{\partial^2 u_3}{\partial y_3^2} + 2\frac{\partial^2 u_1}{\partial y_1 \partial y_3} + 2\frac{\partial^2 u_2}{\partial y_2 \partial y_3} \end{pmatrix}_{\mathbf{y}=\mathbf{X}(t)} + \mathcal{O}(R^4), \tag{3.33}$$

as $R \to 0$

Proof. Using the Taylor expansion near $\mathbf{y} = \mathbf{X}(t)$, we have for $\mathbf{y} \in \mathcal{S}(\mathbf{X}(t), R)$

$$\begin{aligned} \mathbf{u}(\mathbf{y}) - \mathbf{u}(\mathbf{X}(t)) &= \sum_{\ell=1}^{3} \frac{\partial \mathbf{u}(\mathbf{X}(t))}{\partial y_\ell}(y_\ell - X_\ell(t)) + \sum_{\ell=1}^{3}\sum_{k=1}^{3} \frac{1}{2}\frac{\partial^2 \mathbf{u}(\mathbf{X}(t))}{\partial y_\ell \partial y_k}(y_\ell - X_\ell(t))(y_k - X_k(t)) \\ &\quad + \sum_{\ell=1}^{3}\sum_{k=1}^{3}\sum_{j=1}^{3} \frac{1}{3}\frac{\partial^3 \mathbf{u}(\mathbf{X}(t))}{\partial y_\ell \partial y_k \partial y_k}(y_\ell - X_\ell(t))(y_k - X_k(t))(y_j - X_j(t)) + \mathcal{O}(R^4) \\ &= \text{linear terms} + \text{quadratic terms} + \text{cubic terms} + \mathcal{O}(R^4). \end{aligned} \tag{3.34}$$

Since $\boldsymbol{A}_R$ is a linear operator, we have

$$\boldsymbol{A}_R[\mathbf{u}(\mathbf{y}) - \mathbf{u}(\mathbf{X}(t))] = \boldsymbol{A}_R[\text{linear terms}] + \boldsymbol{A}_R[\text{quadratic terms}] + \boldsymbol{A}_R[\text{cubic terms}] + \mathcal{O}(R^4).$$

Utilizing the symmetry of the integration domain, we have that

$$\int_{\mathcal{S}(\mathbf{X}(t),\,R)} \frac{\mathbf{y} - \mathbf{X}(t)}{R}\left\{(y_\ell - X_\ell(t))\mathbf{C} \cdot \frac{\mathbf{y} - \mathbf{X}(t)}{R}\right\} \mathrm{d}A = 0,$$

for all $\ell = 1,2,3$ and all constant vectors $\mathbf{C}$, from which it follows $\boldsymbol{A}_R[\text{linear terms}] = \mathbf{0}$. Similarly,

$$\int_{\mathcal{S}(\mathbf{X}(t),\,R)} \frac{\mathbf{y} - \mathbf{X}(t)}{R}\left\{(y_\ell - X_\ell(t))(y_j - X_j(t))(y_k - X_k(t))\mathbf{C} \cdot \frac{\mathbf{y} - \mathbf{X}(t)}{R}\right\} \mathrm{d}A = 0$$

for all $\ell, j, k = 1,2,3$ and all constant vectors $\mathbf{C}$, from which it follows $\boldsymbol{A}_R[\text{cubic terms}] = \mathbf{0}$. Consequently, we deduce

$$\boldsymbol{A}_R[\mathbf{u}(\mathbf{y}) - \mathbf{u}(\mathbf{X}(t))] = \boldsymbol{A}_R[\text{quadratic terms}] + \mathcal{O}(R^4), \tag{3.35}$$

where the quadratic terms given in equation (3.34) will result in non-zero contributions. We consider the action of $\boldsymbol{A}_R$ on a generic vector with strictly quadratic terms, of the form

$$\mathbf{B} = \sum_{\ell=1}^{3}\sum_{j=1}^{3} \mathbf{B}_{\ell,j}(y_\ell - X_\ell(t))(y_j - X_j(t)), \tag{3.36}$$

where the $\mathbf{B}_{\ell,j}$ are constant in $\mathbf{y}$. We have that

$$\begin{aligned}\boldsymbol{A}_R[\mathbf{B}] &= \frac{3}{4\pi R^2}\int_{S(\mathbf{X}(t),R)} \frac{\mathbf{y}-\mathbf{X}(t)}{R}\left\{\left[\sum_{\ell=1}^{3}\sum_{j=1}^{3}\mathbf{B}_{\ell,j}(y_\ell - X_\ell(t))(y_j - X_j(t))\right]\cdot\frac{\mathbf{y}-\mathbf{X}(t)}{R}\right\}\mathrm{d}A \\ &= \frac{3}{4\pi R^2}\sum_{\ell=1}^{3}\sum_{j=1}^{3}\int_{S(\mathbf{X}(t),R)}\frac{\mathbf{y}-\mathbf{X}(t)}{R}(y_\ell - X_\ell(t))(y_j - X_j(t))\left\{\mathbf{B}_{\ell,j}\cdot\frac{\mathbf{y}-\mathbf{X}(t)}{R}\right\}\mathrm{d}A \\ &= \frac{R^2}{5}\begin{pmatrix} 3B_{1,1;1}+B_{2,2;1}+B_{3,3;1}+B_{1,2;2}+B_{2,1;2}+B_{1,3;3}+B_{3,1;3} \\ B_{1,2;1}+B_{2,1;1}+B_{1,1;2}+3B_{2,2;2}+B_{3,3;2}+B_{2,3;3}+B_{3,2;3} \\ B_{1,3;1}+B_{3,1;1}+B_{2,3;2}+B_{3,2;2}+B_{1,1;3}+B_{2,2;3}+3B_{3,3;3}\end{pmatrix}. \end{aligned} \tag{3.37}$$

Here by $B_{\ell,j;k}$, we mean the kth component ($k = 1,2,3$) of $\mathbf{B}_{\ell,j}$. Comparing the general vector $\mathbf{B}$ with the form of the quadratic terms in the expansion (3.34) for $\mathbf{u}(\mathbf{y}) - \mathbf{u}(\mathbf{X}(t))$, the quadratic terms may be written in the form (3.36) provided

$$B_{\ell,j;k} = \frac{1}{2}\frac{\partial^2 u_k(\mathbf{X}(t))}{\partial y_\ell \partial y_j}\,. \tag{3.38}$$

Since $\mathbf{u}(\mathbf{y})$ is assumed smooth, by Clairaut's Theorem, we can exchange partial derivatives in equation (3.38) to get $B_{\ell,j;k} = B_{j,\ell;k}$ for all $\ell, j = 1,2,3$. Substituting equation (3.38) into equations (3.37) and equation (3.35), we obtain equation (3.33). ∎

Corollary 3.2. *If the flow of solvent particles is governed by a linear velocity field* $\mathbf{u}(\mathbf{y})$, *then the correction term* $\boldsymbol{A}_R[\mathbf{u}(\mathbf{y}) - \mathbf{u}(\mathbf{X})]$ *in equation (3.17) vanishes, in which case the Itô stochastic differential equations (3.1)–(3.2) for the motion of the heavy solute particle has drift term which takes the form*

$$\boldsymbol{\alpha}(\mathbf{X},\mathbf{V}) = -\sqrt{2\pi}\,\mathcal{F}_1\gamma\{\mathbf{V} - \mathbf{u}(\mathbf{X})\} + \mathcal{O}\left(\frac{1}{\sigma_\mu}\right) \quad \text{as} \quad \sigma_\mu \to \infty\,. \tag{3.39}$$

Proof. For any linear flow, equations (3.35) and (3.38) imply $\boldsymbol{A}_R[\mathbf{u}(\mathbf{y}) - \mathbf{u}(\mathbf{X})] = \mathbf{0}$ and the result (3.39) then directly follows from equation (3.17a).

Examples of flows for which Corollary 3.2 is applicable include: (i) uniform flow, $\mathbf{u}(\mathbf{x}) = \mathbf{C}$, where $\mathbf{C}$ is a constant vector; (ii) planar Couette flow, $\mathbf{u}(\mathbf{x}) = (0,0,u\,x_1)^{\mathrm{T}}$, with velocity directed along the x_3 axis and u being a constant; and (iii) generic stagnation flows given in the form $\mathbf{u}(\mathbf{x}) = (u_1\,x_1,\, u_2\,x_2,\, u_3\,x_3)^{\mathrm{T}}$, where the condition $u_1 + u_2 + u_3 = 0$ holds [59,60]. For these flows, Corollary 3.2 implies that the SDEs given by drift and diffusion terms (3.39) are exact, with no finite-size corrections needed. We now provide an example of a quadratic flow, the Poiseuille flow within a circular pipe [61], to illustrate the role of the correction term.

Corollary 3.3. *If the flow of solvent particles is governed by a Poiseuille flow within a pipe of radius* h *taking the form*

$$\mathbf{u}(\mathbf{x}) = \left(0,0,\left(1 - \frac{x_1^2 + x_2^2}{h^2}\right)\overline{u}\right)^{\mathrm{T}}, \tag{3.40}$$

where $\boldsymbol{u}$ *is a constant, then the Itô stochastic differential equations (3.1)–(3.2) for the motion of the heavy solute particle has drift term of the form*

$$\boldsymbol{\alpha}(\mathbf{X},\mathbf{V}) = -\sqrt{2\pi}\,\mathcal{F}_1\gamma\left\{\mathbf{V} - \left(0,0,\left(1 - \frac{2R^2}{5h^2} - \frac{X_1^2 + X_2^2}{h^2}\right)\overline{u}\right)^{\mathrm{T}}\right\} + \mathcal{O}\left(\frac{1}{\sigma_\mu}\right) \tag{3.41}$$

as $\sigma_\mu \to \infty$.

Proof. We have

$$\frac{\partial^2 u_3}{\partial y_1^2} = -\frac{2u}{h^2}, \quad \frac{\partial^2 u_3}{\partial y_2^2} = -\frac{2u}{h^2}, \quad \text{and} \quad \frac{\partial^2 u_3}{\partial y_\ell y_j} = 0 \quad \text{otherwise}.$$

The correction term $\boldsymbol{A}[\mathbf{u}(\mathbf{y}) - \mathbf{u}(\mathbf{X})]$ then reads

royalsocietypublishing.org/journal/rspa Proc. R. Soc. A 480: 20230851

$$\boldsymbol{A}[\mathbf{u}(\mathbf{y}) - \mathbf{u}(\mathbf{X})] = \frac{R^2}{10}\left(0, 0, -\frac{4u}{h^2}\right)^{\mathrm{T}} = -\frac{2R^2u}{5h^2}(0, 0, 1)^{\mathrm{T}}.$$

Using this correction term in equation (3.17a), and noting that there are no higher-order corrections since the flow is exactly quadratic, we obtain equation (3.41). ∎

As our last example in this subsection, we consider a boundary-layer flow over a stretching plate, which admits an exact solution found by Crane [62]. Assume a plate lying on the $x_3 = 0$ plane is stretched along the x_1 axis. Then, in the region $x_1 > 0$, $x_2 \in \mathbb{R}$, $x_3 > 0$, we have the velocity field

$$\mathbf{u}(\mathbf{x}) = \left(\overline{u}\,\frac{x_1}{h_1}\exp\left(-\frac{x_3}{h_3}\right),\ 0,\ -\frac{\overline{u}\,h_3}{h_1}\left[1 - \exp\left(-\frac{x_3}{h_3}\right)\right]\right)^{\mathrm{T}}, \tag{3.42}$$

where u,h_1 and h_3 are positive constants.

Corollary 3.4. *If the flow of solvent particles is governed by a boundary-layer flow described by the solution of Crane (3.42), then the Itô stochastic differential equations (3.1)–(3.2) for the motion of the heavy solute particle has drift term of the form*

$$\boldsymbol{\alpha}(\mathbf{X}, \mathbf{V}) = -\sqrt{2\pi}\,\mathcal{F}_1\gamma\left\{\mathbf{V} - \overline{u}\begin{pmatrix}\left[1 + \dfrac{R^2}{10h_3^2}\right]\dfrac{X_1(t)}{h_1}\,\mathrm{e}^{-X_3(t)/h_3} \\ 0 \\ \dfrac{h_3}{h_1}\left[1 + \dfrac{R^2}{10h_3^2}\right]\mathrm{e}^{-X_3(t)/h_3} - \dfrac{h_3}{h_1}\end{pmatrix}\right\} + \mathcal{O}\left(\frac{1}{\sigma_\mu}\right) + \mathcal{O}(R^4) \tag{3.43}$$

as $R \to 0$ *and* $\sigma_\mu \to \infty$.

Proof. Differentiating the components of equation (3.42), we obtain

$$\frac{\partial^2 u_1}{\partial y_1 \partial y_3} = -\frac{u}{h_1 h_3}\mathrm{e}^{-y_3/h_3}, \qquad \frac{\partial^2 u_1}{\partial y_3^2} = \frac{u}{h_1 h_3^2}\,y_1\,\mathrm{e}^{-y_3/h_3}, \qquad \frac{\partial^2 u_3}{\partial y_3^2} = \frac{u}{h_1 h_3}\,\mathrm{e}^{-y_3/h_3},$$

while all other second-order partial derivatives are zero. Using Theorem 3.5, we have

$$\boldsymbol{A}_R[\mathbf{u}(\mathbf{y}) - \mathbf{u}(\mathbf{X})] + \mathcal{O}(R^4) = \frac{R^2}{10}\begin{pmatrix}\dfrac{\partial^2 u_1}{\partial y_3^2} \\ 0 \\ 3\dfrac{\partial^2 u_3}{\partial y_3^2} + 2\dfrac{\partial^2 u_1}{\partial y_1 \partial y_3}\end{pmatrix}_{\mathbf{y} = \mathbf{X}(t)} = \frac{R^2\,\overline{u}\,\mathrm{e}^{-X_3(t)/h_3}}{10h_1h_3}\begin{pmatrix}X_1(t)/h_3 \\ 0 \\ 1\end{pmatrix}.$$

Substituting into equation (3.17a), we obtain equation (3.43). ∎

4. Simulations in a co-moving frame

In this section, we validate the results of §3 by performing illustrative computer simulations. One way to compare the theory and simulation is to numerically approximate the scale factors for the drift ($\chi_1(\theta)$) and diffusion ($\chi_2(\theta)$) terms in the motion of a heavy particle predicted by the theory, assuming the velocities of solvent particles are sampled according to the generalized Gaussian distribution (3.26). Since we want to estimate the scale factors $\chi_1(\theta)$ and $\chi_2(\theta)$, we need to perform simulations over sufficiently long time, averaging over many collisions with solvent particles. Our simulations consider more than 10^8 solvent particles and the system evolves for more than 10^8 time steps of length Δt. In particular, a direct simulation of such a large system would be computationally intensive.

To design an efficient computational scheme, we only explicitly simulate the behaviour of approximately 900 particles at any one time, because our computer simulations perform in a

co-moving cubic frame of length L that is centred at $\mathbf{X}(t)$, i.e. solvent particles are explicitly simulated in the cubic box

$$\mathbf{X}(t) + \left[-\frac{L}{2}, \frac{L}{2}\right] \times \left[-\frac{L}{2}, \frac{L}{2}\right] \times \left[-\frac{L}{2}, \frac{L}{2}\right], \tag{4.1}$$

while we assume that the solvent particles are distributed according to the spatial Poisson process with density λ_μ given by equation (1.3) and their velocities are distributed according to $f_\mu(\mathbf{v}, \mathbf{u})$ given by equation (2.1). Simulation in a co-moving frame was introduced in Gunaratne *et al*. [9] for the case without flow, i.e. for $\mathbf{u} \equiv \mathbf{0}$ and for the Gaussian distribution (1.4). Here, we extend this approach to the case of general flow, i.e. for $\mathbf{u} \neq \mathbf{0}$ and for general velocity distribution (2.1) as Algorithm [A1]–[A6] in table 3, which presents an update of the state of the system from time t to time $t + \Delta t$, where the time step Δt is assumed to be small enough so that at most one collision happens during the time interval $[t, t + \Delta t]$. Algorithm [A1]–[A6] evolve the positions and velocities of $N(t)$ solvent particles, where $N(t)$ will fluctuate around the value 900 in our illustrative simulations in co-moving frame (4.1).

The initial position and velocity of the heavy particle are $X(0) = 0$ and $V(0) = 0$, respectively. The positions of solvent particles are initialized in the exterior of the heavy particle according to a spatial Poisson process with density λ_μ in our simulation domain (4.1). The initial velocities of solvent particles are drawn from the distribution $f_\mu(\mathbf{v}, \mathbf{u})$ given by equation (2.1).

We first update the positions in Step [A1] over the time interval $[t, t + \Delta t]$ using the free-flight equations

$$\widehat{\mathbf{X}}(t + \Delta t) = \mathbf{X}(t) + \mathbf{V}(t)\,\Delta t, \tag{4.2}$$

$$\widehat{\mathbf{x}}_j(t + \Delta t) = \mathbf{x}_j(t) + \mathbf{v}_j(t)\,\Delta t, \tag{4.3}$$

where $j = 1,2, \ldots, N(t)$. In Step [A2], we update the velocities of the solvent particles which did not collide with the heavy particle by a discretized version of equation (2.4), that is, by

$$\mathbf{v}_j(t + \Delta t) = \mathbf{v}_j(t) + \big(\nabla \mathbf{u}(\mathbf{x}_j(t))\big)\mathbf{v}_j(t)\,\Delta t, \tag{4.4}$$

where $\nabla \mathbf{u}(\mathbf{x}_j(t))$ means that we evaluate $\nabla \mathbf{u}$ at the position $\mathbf{x}_j(t)$ of the jth particle at time t. This means that equations (4.3) and (4.4) form the forward Euler discretization of ODEs (2.4). To formulate Algorithm [A1]–[A6], we assume that Δt is chosen small enough so that at most one collision happens during the time interval $[t, t + \Delta t]$. To determine the colliding particle, we evaluate the condition

$$\left\| \widehat{\mathbf{x}}_j(t + \Delta t) - \widehat{\mathbf{X}}(t + \Delta t) \right\|_2 < R,$$

for all solvent particles in Steps [A2] and [A3]. If the particle did collide, then we do not use equation (4.4) during the collision time-step. In Step [A4], we update the position and velocity of the co-moving frame to $\mathbf{X}(t + \Delta t)$ and

$$\mathbf{V}_{\mathrm{f}} = \frac{\mathbf{X}(t + \Delta t) - \mathbf{X}(t)}{\Delta t}. \tag{4.5}$$

We update $N(t)$ by removing the solvent particles which are outside of the simulation domain. In Step [A5], we calculate the number of particles which entered the simulation domain during the time interval $[t, t + \Delta t]$ through each corresponding side of the co-moving frame. The mean number of particles entering through the left (−) and right (+) of the ith side is denoted as

$$p_i^{\pm}(\mathbf{V}_i), \qquad \text{for} \quad i = 1,2,3, \tag{4.6}$$

and it is calculated for each considered distribution in §4*a*, where we also specify the distributions of the initial positions $\mathbf{x}_{\mathrm{new}}$ and velocities $\mathbf{v}_{\mathrm{new}}$ of the introduced solvent particles. Since our calculation of incoming probabilities (4.6) uses boundaries equal to infinite planes, some

Table 3. One iteration of the simulation algorithm in a co-moving frame.

[A1]	Update the positions of the solute and solvent particles by calculating their free-flight positions (4.2)–(4.3).
[A2]	Update the velocities of all solvent particles for which the free-flight position (4.3) lies outside the radius of the solute particle by equation equation (4.4).
[A3]	If the free-flight position (4.3) of a solvent particle lies within the radius of the solute particle, reverse the trajectories of the solvent and the solute particles by time $\tau < \Delta t$ such that they are just touching. Calculate post-collision velocities by equations (1.1)–(1.2) and further update their new positions by moving forward by time τ. Otherwise, each free-flight position (4.3) is accepted as the particle's position at time $t + \Delta t$.
[A4]	Update $N(t)$ by removing those solvent particles which lie outside of the co-moving frame (4.1) centred at new position of the solute particle, $\mathbf{X}(t + \Delta t)$, from the simulation. Calculate the velocity of the co-moving frame, $\mathbf{V}_f$, over the time interval $[t, t + \Delta t]$ by equation (4.5).
[A5]	Generate six Poisson distributed random numbers N_i^- and N_i^+, for $i = 1, 2, 3$, with means $p_i^-(\mathbf{V}_f)$ and $p_i^+(\mathbf{V}_f)$, respectively. For each side i, generate N_i^- and N_i^+ proposed positions and velocities of new solvent particles. For each proposed new particle position $\mathbf{x}_{new}$ with velocity $\mathbf{v}_{new}$, generate a random number r uniformly distributed in interval $(0, 1)$. If $r < h_{acc}(\mathbf{x}_{new}, \mathbf{v}_{new})$, where $h_{acc}(\mathbf{x}_{new}, \mathbf{v}_{new})$ is given by equation (4.7), then increase $N(t)$ by 1 and initialize the new solvent particle at the proposed position $\mathbf{x}_{new}$ with velocity $\mathbf{v}_{new}$.
[A6]	Continue with Step [A1] using time $t = t + \Delta t$.

regions are counted twice or three times in our derivation. Therefore, in Step [A5], we consider the proposed sampled position $\mathbf{x}_{new}$ and velocity $\mathbf{v}_{new}$ of each incoming particle at time $t + \Delta t$, calculate its previous position at time t by

$$\mathbf{y} = \mathbf{x}_{new} - \mathbf{v}_{new}\,\Delta t,$$

and define the acceptance probability by

$$h_{acc}(\mathbf{x}_{new}, \mathbf{v}_{new}) = \begin{cases} 1, & \text{for } \mathbf{y} - \mathbf{X}(t) \in \mathcal{Y}_1; \\ 1/2, & \text{for } \mathbf{y} - \mathbf{X}(t) \in \mathcal{Y}_2; \\ 1/3, & \text{for } \mathbf{y} - \mathbf{X}(t) \in \mathcal{Y}_3, \end{cases} \tag{4.7}$$

where $\mathcal{Y}_j \subset \mathbb{R}^3$ is the region of the space which consists of points which have exactly j of their coordinates outside of the interval $[-L/2, L/2]$. The acceptance probability (4.7) takes into account that regions $\mathcal{Y}_2$ and $\mathcal{Y}_3$ are counted twice and three times, respectively, in our derivation of boundary conditions of co-moving frame (4.1). Regions $\mathcal{Y}_1$ and $\mathcal{Y}_2$ are illustrated in the schematic of our co-moving frame in figure 1*a* with some of their boundaries highlighted by the magenta and green shading. Region $\mathcal{Y}_3$ is next to the corners of the cube consisting of points, which have all coordinates outside of the interval $[-L/2, L/2]$.

(a) Distributions of particles entering the co-moving frame in Step [A5]

To apply Algorithm [A1]–[A6], we need to calculate the number, positions and velocities of incoming solvent particles in Step [A5]. We will study the behaviour at the boundary side

$$\left\{X_1(t) - \frac{L}{2}\right\} \times \left[X_2(t) - \frac{L}{2}, X_2(t) + \frac{L}{2}\right] \times \left[X_3(t) - \frac{L}{2}, X_3(t) + \frac{L}{2}\right], \tag{4.8}$$

in Theorem 4.1, where this boundary is approximated as the plane $\{X_1(t) - L/2\} \times \mathbb{R}^2$ dividing the space $\mathbb{R}^3$ into two half-spaces approximating the exterior and the interior of the co-moving frame (4.1). We consider those particles which are not explicitly simulated at time t (because

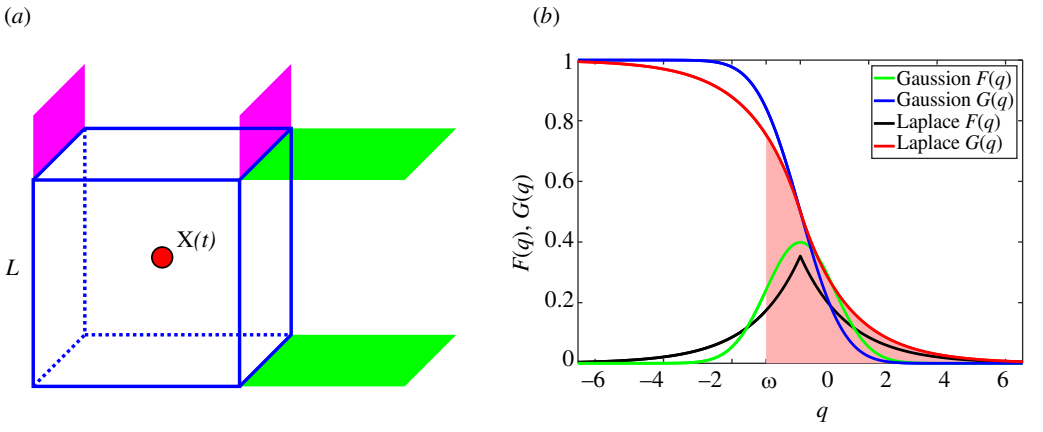

Figure 1. (*a*) Schematic of the co-moving frame (4.1) is shown as the blue cube with centre $\mathbf{X}(t)$ and size L. Some parts of region $\mathcal{Y}_1$ (used in equation (4.7)) are between the magenta shaded planes and between the green shaded planes, while the region (next to the edge) bounded by the green and magenta planes is a part of $\mathcal{Y}_2$. (*b*) Functions $\mathcal{F}(q)$ and $\mathcal{G}(q)$ given by equation (4.14) and listed in table 5. The shaded part illustrates the probability distribution (4.19) for $\omega = -1$.

they are outside of the co-moving frame at time t), but they have to be included in the simulation at time $t + \Delta t$, because they entered the co-moving frame at time $t + \Delta t$. The results for the five other sides of the co-moving frame (4.1) can be obtained in the same way.

Theorem 4.1. *Let $\Delta t > 0$. Let us assume that solvent particles are distributed according to the Poisson distribution with density λ_μ in the half space $(-\infty, X_1(t) - L/2) \times \mathbb{R}^2$; their initial velocities are distributed according to $f_\mu(\mathbf{v}, \mathbf{u})$ and there are no particles in the half space $(X_1(t) - L/2, \infty) \times \mathbb{R}^2$ at time t. Then, the positions $\mathbf{x}$ and velocities $\mathbf{v}$ of solvent particles are distributed at time $t + \Delta t$ according to*

$$\begin{aligned} g(\mathbf{x}, \mathbf{v}; \Delta t) = {} & H(X_1(t) - L/2 - x_1 + v_1 \Delta t)\, \lambda_\mu f_\mu(\mathbf{v}, \mathbf{u}) \\ & - H\big(X_1(t) - L/2 - x_1\big)\, \lambda_\mu \nabla_{\mathbf{u}} f_\mu(\mathbf{v}, \mathbf{u})(\nabla \mathbf{u})\mathbf{v}\, \Delta t + O\big((\Delta t)^2\big), \end{aligned} \tag{4.9}$$

where $H(\,\cdot\,)$ is the Heaviside step function and

$$\nabla_{\mathbf{u}} f_\mu(\mathbf{v}, \mathbf{u})(\nabla \mathbf{u})\mathbf{v} \equiv \sum_{j,\ell=1}^{3} \frac{\partial f_\mu}{\partial u_j}(\mathbf{v}, \mathbf{u}(\mathbf{x})) \frac{\partial u_j}{\partial x_\ell}(\mathbf{x})\, v_\ell\,.$$

The marginal distribution of the positions $\mathbf{x}$ of solvent particles at time $t = \Delta t$ is then

$$\begin{aligned} \varrho(\mathbf{x}; \Delta t) = {} & \lambda_\mu \int_{(L/2 + x_1 - X_1(t))/\Delta t}^{\infty} \int_{-\infty}^{\infty} \int_{-\infty}^{\infty} f_\mu(\mathbf{v}, \mathbf{u})\, \mathrm{d}v_3\, \mathrm{d}v_2\, \mathrm{d}v_1 \\ & - H\Big(X_1(t) - L/2 - x_1\Big) \lambda_\mu \Delta t \int_{\mathbb{R}^3} \nabla_{\mathbf{u}} f_\mu(\mathbf{v}, \mathbf{u})(\nabla \mathbf{u})\mathbf{v}\, \mathrm{d}\mathbf{v} + O\Big((\Delta t)^2\Big)\,. \end{aligned} \tag{4.10}$$

Proof. Solvent particles which have their position $\mathbf{x} = (x_1, x_2, x_3)^{\mathrm{T}}$ and velocity $\mathbf{v} = (v_1, v_2, v_3)^{\mathrm{T}}$ at time $t + \Delta t$ were previously (at time t) with the position and velocity, which we denote by $\mathbf{x}_{\mathrm{old}} = (x_{1,\,\mathrm{old}}, x_{2,\,\mathrm{old}}, x_{3,\,\mathrm{old}})^{\mathrm{T}}$ and $\mathbf{v}_{\mathrm{old}} = (v_{1,\,\mathrm{old}}, v_{2,\,\mathrm{old}}, v_{3,\,\mathrm{old}})^{\mathrm{T}}$. There will be non-zero solvent particles with velocity $\mathbf{v}$ at point $\mathbf{x}$ at time $t + \Delta t$ provided that $x_{1,\,\mathrm{old}} < X_1(t) - L/2$ which implies that

$$g(\mathbf{x}, \mathbf{v}; \Delta t) = H(X_1(t) - L/2 - x_{1,\,\mathrm{old}})\, \lambda_\mu f_\mu(\mathbf{v}, \mathbf{u}(\mathbf{x}_{\mathrm{old}}))\,. \tag{4.11}$$

Using equations (4.3) and (4.4), we have

$$\begin{aligned} x_{1,\,\mathrm{old}} &= x_1 - v_{1,\,\mathrm{old}}\, \Delta t, \\ v_{1,\,\mathrm{old}} &= v_1 - (\nabla \mathbf{u}(\mathbf{x}_{\mathrm{old}}))\mathbf{v}_{\mathrm{old}}\, \Delta t, \end{aligned}$$

Substituting into equation (4.11), we obtain

$$g(\mathbf{x}, \mathbf{v}; \Delta t) = H\big(X_1(t) - L/2 - x_1 + v_1 \Delta t\big)\, \lambda_\mu\, f_\mu(\mathbf{v}, \mathbf{u}(\mathbf{x} - \mathbf{v}\Delta t)) + O\big((\Delta t)^2\big).$$

Using the Taylor expansion, we obtain equation (4.9) to order $O((\Delta t)^2)$. The marginal distribution of the positions $\mathbf{x}$ of solvent particles at time $t + \Delta t$ can then be obtained by integrating $g(\mathbf{x}, \mathbf{v}; \Delta t)$ over all possible velocities, giving

$$\varrho(\mathbf{x}; \Delta t) = \int_{\mathbb{R}^3} g(\mathbf{x}, \mathbf{v}; \Delta t)\, \mathrm{d}\mathbf{v}\,.$$

Using the formula for $g(\mathbf{x}, \mathbf{v}; \Delta t)$ given by equation (4.9), we obtain equation (4.10). ∎

To apply Theorem 4.1 to the left side in the first direction (4.8) of the co-moving frame (4.1), we identify the co-moving frame (4.1) at time $t + \Delta t$ with the semi-infinite cuboid

$$\mathbf{X}(t + \Delta t) + \left[-\frac{L}{2}, \infty\right) \times \left[-\frac{L}{2}, \frac{L}{2}\right] \times \left[-\frac{L}{2}, \frac{L}{2}\right]. \tag{4.12}$$

Then, the mean number of particles entering through the left side in the first direction (4.8) of the co-moving frame can be calculated as the average number of particles in the semi-infinite cuboid (4.12) by integrating

$$p_1^-(\mathbf{V}_f) = \int_{[X_1(t+\Delta t) - L/2, \infty) \times [0, L]^2} \varrho(\mathbf{x}; \Delta t)\, \mathrm{d}\mathbf{x}, \tag{4.13}$$

where $\varrho(\mathbf{x}; \Delta t)$ is given by equation (4.10) and we have used that the integration domain can be translated in the second and third directions without changing the integral. To evaluate integrals in equations (4.10) and (4.13), we will assume that the velocity distribution $f_\mu(\mathbf{v}, \mathbf{u}) = F_\mu(\mathbf{v} - \mathbf{u})$ in equation (2.1) is given in the product form (2.3) and $\mathbf{u}$ is a constant vector (uniform flow). We define

$$\mathcal{G}(z) = \int_z^\infty \mathcal{F}(q)\, \mathrm{d}q \qquad \text{and} \qquad \mathcal{K}(z) = \int_z^\infty \mathcal{G}(q)\, \mathrm{d}q\,. \tag{4.14}$$

Since $\nabla \mathbf{u}$ is a zero matrix for uniform flow $\mathbf{u}$, equation (4.10) simplifies as follows:

$$\varrho(\mathbf{x}; \Delta t) \equiv \varrho(x_1; \Delta t) = \lambda_\mu\, \mathcal{G}\left(\frac{L + 2\,x_1 - 2\,X_1(t) - 2\,u_1\,\Delta t}{2\,\sigma_\mu\,\Delta t}\right). \tag{4.15}$$

Substituting into equation (4.13), we get

$$p_1^-(\mathbf{V}_f) = \lambda_\mu\, L^2\, \sigma_\mu\, \Delta t\ \mathcal{K}\left(\frac{V_{f,1} - u_1}{\sigma_\mu}\right),$$

where $\mathbf{V}_f = (V_{f,1}, V_{f,2}, V_{f,3})^{\mathrm{T}}$ is the frame velocity defined by equation (4.5) and $\mathbf{u}$ is the underlying flow vector field. Using symmetry, we can then express the numbers of particles entering the co-moving frame during one time step through each side by

$$p_i^{\pm}(\mathbf{V}_f) = \lambda_\mu\, L^2\, \sigma_\mu\, \Delta t\ \mathcal{K}\left(\pm\frac{u_i - V_{f,i}}{\sigma_\mu}\right), \qquad \text{for} \quad i = 1, 2, 3. \tag{4.16}$$

These numbers are then used in Step [A5] of Algorithm [A1]–[A6] in table 3. The distribution of the initial positions of the incoming particle is proportional to equation (4.15) which is restricted to the semi-infinite cuboid (4.12). Since equation (4.15) only depends on x_1, the distribution of the second and third coordinates is uniform in $[X_2(t + \Delta t) - L/2, X_2(t + \Delta t) + L/2]$ and $[X_3(t + \Delta t) - L/2, X_3(t + \Delta t) + L/2]$, respectively, while the first coordinate can be sampled as

$$x_1 = X_1(t + \Delta t) - L/2 + \zeta\, \sigma_\mu\, \Delta t\,, \tag{4.17}$$

where ζ is the dimensionless distance (expressed in units of $\sigma_\mu \Delta t$) from the boundary (4.8) at time $t + \Delta t$. Using equation (4.15), we can sample ζ according to a distribution proportional to

$$\mathcal{G}\left(\zeta + \frac{V_{\backslash \text{scriptsize f, 1}} - u_1}{\sigma_\mu}\right), \qquad \text{for} \quad \zeta > 0.$$

Using symmetry, the distances of particles entering the co-moving frame through each of its sides are sampled according to distributions proportional to

$$\mathcal{G}\left(\zeta \pm \frac{u_i - V_{\text{f},i}}{\sigma_\mu}\right), \qquad \text{for} \quad \zeta > 0. \tag{4.18}$$

To sample random numbers from distributions (4.18), we will use the acceptance–rejection Algorithm [S1]–[S4] listed in table 4.

This is a generalization of the acceptance–rejection algorithms that were previously used for simulations with Maxwell–Boltzmann statistics [8,9]. In the case of the distributions (4.18), we need to sample random numbers according to the probability distribution

$$p(\zeta; \omega) = \frac{\mathcal{G}(\zeta + \omega)}{\mathcal{K}(\omega)}, \qquad \text{for} \quad \zeta > 0, \tag{4.19}$$

where $\omega \in \mathbb{R}$ is a parameter. This distribution is illustrated in figure 1*b* using the pink shading for $\omega = -1$ and $\mathcal{F}$ being the Laplace distribution.

The algorithm in table 4 samples random numbers according to the distribution (4.19) by generating an exponentially distributed random number η_3 with mean $a_1(\omega)$, which is a parameter of the method satisfying

$$p(\zeta; \omega) \le \frac{1}{a_2(\omega)\, \mathcal{K}(\omega)} \exp\left[-\frac{\zeta}{a_1(\omega)}\right] \qquad \text{for all} \quad \zeta > 0, \tag{4.20}$$

where $a_2(\omega)$ is the second parameter of the method. Substituting equation (4.19) into equation (4.20), we get

$$a_2(\omega)\, \mathcal{G}(\zeta + \omega) \exp\left[\frac{\zeta}{a_1(\omega)}\right] \le 1 \qquad \text{for all} \quad \zeta > 0. \tag{4.21}$$

The inequality (4.21) can always be satisfied for some choices of parameters $a_1(\omega)$ and $a_2(\omega)$, because $\mathcal{G}$ is exponentially decreasing for large values of ζ as can be seen in figure 1*b*. In practice, we have to choose $a_1(\omega)$ and $a_2(\omega)$ to have a relatively high acceptance probability which is the number on the left-hand side of condition (4.21). Since our exponentially distributed random number η_3 is obtained in Step [S3] as $\eta_3 = -a_1(\omega) \log(\eta_1)$, we can substitute this into the left-hand side of condition (4.21) for ζ to get the acceptance probability in Step [S4] as

$$\frac{a_2(\omega)\, \mathcal{G}(\eta_3 + \omega)}{\eta_1}. \tag{4.22}$$

A relatively high acceptance probability gives an efficient algorithm, because it decreases the number of repeats of Steps [S2]–[S4] in table 4. Since η_1 is uniformly distributed in Step [S2] and $\eta_3 = -a_1(\omega) \log(\eta_1)$, we can substitute into equation (4.22) to get the probability that the algorithm [S2]–[S4] finishes in one iteration as

$$\int_0^1 \frac{a_2(\omega)\, \mathcal{G}(-a_1(\omega) \log(s) + \omega)}{s}\, \mathrm{d}s = \int_\omega^\infty \frac{a_2(\omega)}{a_1(\omega)}\, \mathcal{G}(\zeta)\, \mathrm{d}\zeta = \frac{a_2(\omega)\, \mathcal{K}(\omega)}{a_1(\omega)}. \tag{4.23}$$

An appropriate choice of the parameters $a_1(\omega)$ and $a_2(\omega)$ will depend on our choice of $\mathcal{F}$. In our illustrative simulations, we will use two of the functions $\mathcal{F} : \mathbb{R} \to [0, \infty)$ which have been listed

Table 4. Acceptance–rejection algorithm for sampling random numbers according to the probability distribution $p(\zeta;\omega)$ given by equation (4.19).

[S1]	Calculate $a_1(\omega)$ and $a_2(\omega)$ that satisfy the inequality (4.21) for all $\zeta > 0$.
[S2]	Generate two random numbers η_1 and η_2 uniformly distributed in the interval (0,1).
[S3]	Compute an exponentially distributed random number η_3 by $\eta_3 = -a_1(\omega)\log(\eta_1)$.
[S4]	If $\eta_1\eta_2 < a_2(\omega)\,\mathcal{G}(\eta_3+\omega)$, then choose η_3 as a sample from the probability distribution (4.19). Otherwise, go to Step [S2] of the algorithm.

in table 1 in §3, namely, the Gaussian (Maxwell–Boltzmann statistics) and Laplace distributions. For these distributions, the integrals $\mathcal{G}$ and $\mathcal{K}$ defined by equation (4.14) can be evaluated and are listed in table 5 together with the choices of $a_1(\omega)$ and $a_2(\omega)$, which we use in our simulations. However, any choice of $a_1(\omega)$ and $a_2(\omega)$ will lead to correct sampling of random numbers by the Algorithm [S1]–[S4] provided that they satisfy the inequality (4.21) for all $\zeta > 0$. Finally, we need a method for sampling velocities of particles introduced into the simulation in Step [A5] according to distribution (4.9). In the case of a velocity distribution $f_\mu(\mathbf{v},\mathbf{u}) = F_\mu(\mathbf{v}-\mathbf{u})$ taking the form of a product as in equation (2.3) and $\mathbf{u}$ being a constant vector (uniform flow), this simplifies to sampling the first coordinate of the incoming velocity of the particle entering through the first side according to the truncated distribution proportional to

$$\mathcal{F}\left(\frac{v_1-u_1}{\sigma_\mu}\right) \quad \text{restricted to the subdomain} \quad v_1 > \frac{x_1 + L/2 - X_2(t)}{\Delta t}, \tag{4.24}$$

while the second and third coordinate of the velocity, v_2 and v_3, are sampled according to untruncated distributions $\mathcal{F}(v_j/\sigma_\mu)/\sigma_\mu$, for $j = 2,3$. Using equation (4.17) and symmetry, the ith coordinates of velocities of particles entering the co-moving frame through the ith left and right sides are sampled according to distributions proportional to

$$\mathcal{F}\left(\frac{v_i-u_i}{\sigma_\mu}\right) \quad \text{restricted to the subdomain} \quad v_i > \zeta\sigma_\mu + V_{\mathrm{f},i}, \tag{4.25}$$

and

$$\mathcal{F}\left(\frac{v_i-u_i}{\sigma_\mu}\right) \quad \text{restricted to the subdomain} \quad v_i < -\zeta\sigma_\mu + V_{\mathrm{f},i}, \tag{4.26}$$

respectively. An appropriate choice of the algorithm for sampling random numbers according to truncated distributions (4.25)–(4.26) will depend on the choice of $\mathcal{F}$, and it is provided for specific distributions in §4b.

(b) Illustrative simulations for Gaussian and Laplace distributions

In figure 2*a*, we present a trajectory of the solute particle calculated by Algorithm [A1]–[A6] and visualized as the red line over a relatively short (dimensionless) time interval $t \in [0,10]$. In this simulation, we use the uniform flow $\mathbf{u} = (1,0,0)^{\mathrm{T}}$ with the dimensionless parameters

$$D = \gamma = m = R = 1, \qquad \Delta t = 10^{-5}, \qquad M = 10^4, \qquad L = 4, \tag{4.27}$$

and the Gaussian distribution for $\mathcal{F}(q)$. In particular, we use the formulas for $a_1(\omega)$ and $a_2(\omega)$ for the Gaussian distribution listed in table 5. To justify these choices, we note that in the case of $\omega \geq 0$, the formulas for $a_1(\omega)$ and $a_2(\omega)$ in table 5 imply that condition (4.21) can be rewritten as

Table 5. Functions $\mathcal{G}$ and $\mathcal{K}$ defined by equation (4.14) and parameters $a_1(\omega)$ and $a_2(\omega)$ satisfying the inequality (4.21) for some marginal density functions $\mathcal{F}$ introduced in table 1.

	Gaussian distribution	Laplace distribution
$\mathcal{F}(q)$	$\frac{1}{\sqrt{2\pi}}\exp\left(-\frac{q^2}{2}\right)$	$\frac{1}{2\sqrt{2}}\exp\left(-\frac{\lvert q\rvert}{\sqrt{2}}\right)$
$\mathcal{G}(q)$	$\frac{1}{2}\operatorname{erfc}\left(\frac{q}{\sqrt{2}}\right)$	$\sqrt{2}\,\mathcal{F}(q)\operatorname{sign}(q)+H(-q) = \begin{cases}\frac{1}{2}\exp\left(-\frac{\lvert q\rvert}{\sqrt{2}}\right), & \text{for } q\geq 0;\\ 1-\frac{1}{2}\exp\left(-\frac{\lvert q\rvert}{\sqrt{2}}\right), & \text{for } q<0.\end{cases}$
$\mathcal{K}(q)$	$\mathcal{F}(q)-q\,\mathcal{G}(q)$	$2\mathcal{F}(q)+\frac{\lvert q\rvert-q}{2}$
$a_1(\omega)$	$\begin{cases}\frac{\mathcal{G}(\omega)}{\mathcal{F}(\omega)}, & \text{for } \omega\geq 0;\\ \frac{\sqrt{\pi}}{\sqrt{2}}, & \text{for } \omega\leq 0.\end{cases}$	$\sqrt{2}$
$a_2(\omega)$	$\begin{cases}\frac{1}{\mathcal{G}(\omega)}, & \text{for } \omega\geq 0;\\ 2\exp\left(\frac{\omega\sqrt{2}}{\sqrt{\pi}}\right), & \text{for } \omega\leq 0.\end{cases}$	$2\exp\left[\frac{\omega}{\sqrt{2}}\right]$

$$\frac{\mathcal{G}(\zeta+\omega)}{\mathcal{G}(\omega)}\exp\left[\frac{\zeta\,\mathcal{F}(\omega)}{\mathcal{G}(\omega)}\right]\leq 1 \qquad \text{for all} \quad \zeta>0.$$

The left-hand side is equal to 1 for $\zeta=0$, which is the maximum value of the left-hand side for $\zeta\geq 0$, meaning that the condition (4.21) is satisfied. On the other hand, if $\omega<0$, then the formulas for $a_1(\omega)$, $a_2(\omega)$ and $\mathcal{G}(\omega)$ in table 5 for the Gaussian distribution imply that the condition (equation 4.21) can be rewritten as

$$\operatorname{erfc}\left(\frac{\zeta+\omega}{\sqrt{2}}\right)\exp\left[\frac{(\zeta+\omega)\sqrt{2}}{\sqrt{\pi}}\right]\leq 1 \qquad \text{for all} \quad \zeta>0,$$

where the left-hand side is equal to 1 at point $\zeta=-\omega$ and this is the maximum value of the left-hand side for $\zeta\geq 0$, meaning that the condition (4.21) is again satisfied.

Using different formulas of $a_1(\omega)$ and $a_2(\omega)$ for $\omega\geq 0$ and $\omega<0$ improves the acceptance probability (4.23) of Algorithm [S1]–[S4], which can be further improved if we use tabulated functions, see [9] for further discussion. The initial velocity of the introduced solvent particle is sampled according to the truncated Gaussian distribution (4.24) using an acceptance–rejection method presented in the literature [63].

Using our parameter values (4.27), equations (1.3) and (1.5) give

$$\mu=10^4, \qquad \lambda_\mu\approx 14.96, \qquad \sigma_\mu\approx 100. \tag{4.28}$$

In particular, the volume of the co-moving frame available to solvent particles is $L^3-(4/3)\pi R^3$ and it contains around $\lambda_\mu(L^3-(4/3)\pi R^3)\approx 895$ solvent particles on average. The positions of solvent particles in the co-moving frame at time $t=10$ are visualized in figure 2*a* as blue dots.

Figure 2*a* illustrates a relatively short simulation for time $t\in[0,10]$. Next, we increase the simulated time interval to $t\in\left[0,\,2{\times}10^3\right]$ using the same values of parameters (4.27) and implementing Algorithm [A1]–[A6] over $2{\times}10^8$ simulated time-steps. We use uniform flow:

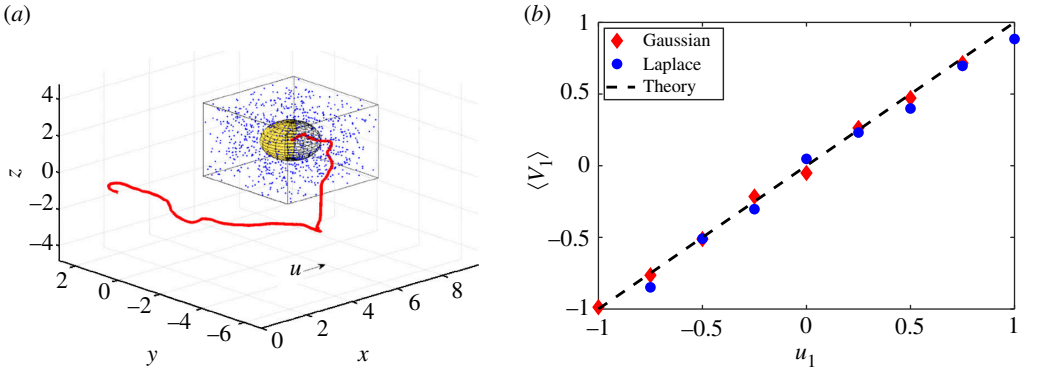

Figure 2. (*a*) The initial trajectory of the large particle for $\mathbf{u} = (1,0,0)^{\mathrm{T}}$ in the time interval $t \in [0,10]$ is visualized as the red line together with the snapshot of positions of solvent particles at time $t = 10$ (blue dots). (*b*) The first coordinate of the average velocity of the large particle, $\langle V_1 \rangle$, plotted as a function of the first coordinate of the fluid flow, u_1.

$$\mathbf{u} = (u_1, 0, 0)^{\mathrm{T}}, \qquad \text{where} \quad u_1 \in \left\{-1, -\frac{3}{4}, -\frac{1}{2}, -\frac{1}{4}, 0, \frac{1}{4}, \frac{1}{2}, \frac{3}{4}, 1\right\}, \tag{4.29}$$

presenting the results of these nine long-time simulations in figure 2*b*. In each simulation, we average the first component of the velocity of the solute particle, $\langle V_1 \rangle$, at every two time steps, so that we average over 10^8 individual data points to calculate $\langle V_1 \rangle$. We plot this quantity in figure 2*b* as a function of u_1, confirming the theoretical result $\langle V_1 \rangle = u_1$.

Our calculated results for the Laplace distribution are also presented in figure 2*b*, where we use the same parameter values (4.27)–(4.28) and the same nine underlying homogeneous flows (4.29) as in the Gaussian case. Using the formulas for $\mathcal{F}$, $\mathcal{G}$, $\mathcal{K}$, $a_1(\omega)$ and $a_2(\omega)$ in table 5 for the Laplace distribution and equation (4.23), we conclude that the Algorithm [S1]–[S4] finishes in one iteration of Steps [S2]–[S4] with probability

$$\frac{a_2(\omega)\,\mathcal{K}(\omega)}{a_1(\omega)} = \begin{cases} 1, & \text{for } \omega \geq 0; \\ \exp\left[\sqrt{2}\,\omega\right] + \sqrt{2}\,|\,\omega\,|\,\exp\left[\dfrac{\omega}{\sqrt{2}}\right], & \text{for } \omega \leq 0. \end{cases}$$

In particular, if $\omega \geq 0$, then the distribution (4.19) is an exponential distribution and our choices of $a_1(\omega)$ and $a_2(\omega)$ listed in table 5 ensure that every exponentially distributed random number calculated in Step [S3] is accepted in Step [S4], so that the algorithm in table 4 finishes in one iteration of Steps [S2]–[S4]. Initial velocities of the introduced solvent particles are sampled according to the truncated Laplace distribution (4.24). To do this, we can sample a random number according to the Laplace distribution and accept it, if it is inside the desired range of values. Such an acceptance–rejection algorithm will have its acceptance probability greater than 1/2, provided that the truncated Laplace distribution (4.24) includes both positive and negative values. If not, then the truncated Laplace distribution becomes an exponential distribution and we do not need to use an acceptance–rejection algorithm.

Figure 3*b* shows the estimated values of coefficients $\chi_1(\theta)$ and $\chi_2(\theta)$ for both Laplace ($\theta = 1$) and Gaussian ($\theta = 2$) distributions. To estimate $\chi_2(\theta)$, we calculate the average:

$$\chi_2(\theta) \approx \left(\frac{1}{2\,D\,\gamma^2}\left\langle \frac{(V_i(t+\Delta t) - V_i(t))^2}{\Delta t}\right\rangle\right)^{1/2} \tag{4.30}$$

during the same long-time simulations of the Algorithm [A1]–[A6], which we have used for figure 2. To estimate $\chi_1(\theta)$, we plot $\langle V_i(t+\Delta t) - V_i(t)\rangle/\Delta t$ as a function of $V_i - u_i$ in figure 3*a* for the simulation with $u_1 = 1$. Using the best linear fit for each coordinate $i = 1,2,3$, we obtain three

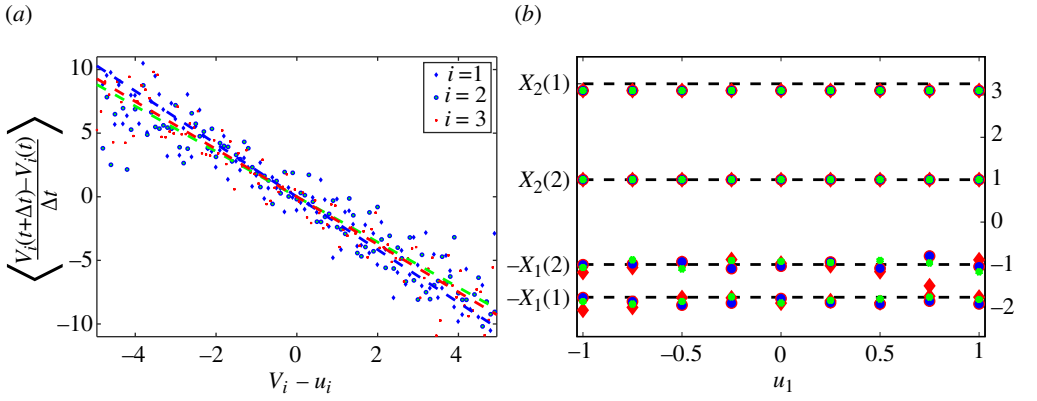

Figure 3. (*a*) Estimation of the coefficient $\chi_1(1)$ defined in equation (3.25) for the simulation of the large particle in flow $\mathbf{u} = (1,0,0)^\mathsf{T}$. We plot $\langle V_i(t+\Delta t) - V_i(t)\rangle/\Delta t$ as a function of $V_i - u_i$, for each coordinate $i = 1,2,3$, and use the best linear fit to estimate the slope, $-\chi_1(1)$, shown in the second panel. (*b*) Coefficients $\chi_1(\theta)$ and $\chi_2(\theta)$ estimated using equation (4.30) from the simulation of the Algorithms [A1]–[A6] for $\theta = 1$ (Laplace distribution) and $\theta = 2$ (Gaussian distribution) as functions of flow velocity u_1.

values of slopes; the resulting estimates of $-\chi_1(\theta)$ are shown in figure 3*b*. All simulation results fall within the $\mathcal{O}(\sigma_\mu^{-1})$ error predicted by the theory.

5. Discussion

We have derived a Langevin-type macroscopic description of a solute particle immersed in a heat bath of light point particles which are subject to a stationary flow. A range of flows and velocity distributions have been considered in §3 and efficient methods for simulating the microscopic system in a co-moving frame have been designed in §4. Our results extend the theory for Brownian motion of a heavy particle to the case where the light heat bath particles follow a prescribed flow. We highlight some key points from our theoretical findings.

The result in Theorem 3.1 provides a general approach for determining the drift and diffusion terms of the Langevin dynamics (3.1)–(3.2) governing the motion of the heavy particle. Many distribution functions (including generalized Gaussian distributions) obey the symmetry property manifesting as the asymptotic scaling (3.15). For heat bath particles obeying such velocity distributions, the approach taken in Theorem 3.2 allows us to simplify the expressions in Theorem 3.1 greatly, resulting in explicit formulas for the drift and diffusion coefficients in the generalized Ornstein–Uhlenbeck process (3.2). The influence of the particular velocity distribution chosen for the heat bath particles manifests through factors which scale the drift and diffusion terms. When the heat bath particle velocities obey a Gaussian distribution (Maxwell–Boltzmann statistics) these scale factors reduce to unity, simplifying to scales common in the literature. When the heat bath particle velocity distribution has a heavy tail, we find that the scale factors are greater than unity (so, faster heat bath particles are more common than in the Gaussian case), while when the heat bath particle velocity distribution is thin-tailed the scale factors are less than unity (hence, slower heat bath particles are more common than in the Gaussian case). These theoretical findings are verified in our numerical simulations in §4.

In addition to the velocity distribution-dependent scale factors discussed above, the drift term in the obtained generalized Ornstein–Uhlenbeck process also depends upon the flow. Prior literature (see, for instance, [33–38]) has generally assumed that the drift term $\boldsymbol{\alpha}$ scales like $\boldsymbol{\alpha} \sim -(\mathbf{V} - \mathbf{u}(\mathbf{X}))$, with a formal derivation for certain linear shear flows appearing more recently in Dobson *et al*. [39]. This approximation is reasonable for heavy particles of negligible size or

for linear flows. However, for heavy particles of finite size in nonlinear flows, this scaling is not complete, and we show via Theorem 3.2 that there are finite-size effects when the heavy particle is large enough to interact with the geometry of the flow. Therefore, the appropriate leading-order scaling for the drift term is $\boldsymbol{\alpha} \sim -(\mathbf{V} - \mathbf{u}(\mathbf{X}) - \mathbf{A}_R)$ where the correction term $\mathbf{A}_R$ is defined by equation (3.18) and depends upon both the flow geometry and the size R of the heavy particle. If the underlying flow of heat bath particles is smooth enough over the problem domain Ω, Theorem 3.5 implies $\mathbf{A}_R = \mathcal{O}(R^2)$ in the particle size R. Therefore, when $\mathcal{O}(R^2)$ contributions are larger than $\mathcal{O}(\sigma_\mu^{-1})$ contributions, it is necessary to include the finite-size correction to the drift term.

There are a number of ways our work might be extended. Regarding the heavy particle, we have assumed a perfect sphere and neglected rotation or angular momentum. Including angular in addition to linear momentum would greatly complicate the governing equations, yet would permit a more realistic view of how a finite-size heavy particle moves within a flow. Inclusion of solid-body motions would also allow for the consideration of non-spherical particles. Furthermore, we have considered one heavy particle immersed within a heat bath of many light particles, and the extension to two or some finite number of heavy particles would be another possible generalization. Collisions with the heat bath particles bias the motion of heavy particles toward the imposed flow, and hence the motion of heavy particles is expected to be along the mean flow yet may differ from this mean flow greatly after interacting with other heavy particles either directly by collisions [64] or indirectly by hydrodynamic interactions through the solvent [65,66]. The co-moving frame algorithm could also be reformulated as an event-based algorithm, where one would replace the time step Δt by the time between collisions, which could be obtained by using equation (2.4) to calculate the potential collision time for each heat bath particle and taking the minimum of them as the next collision time. Depending on $\mathbf{u}$, the next collision time could be calculated exactly or approximately, and in some cases, this could lead to further computational savings. Additional future computational work would include interactions between the light solvent particles and estimating properties of statistical distributions from the underlying molecular dynamics simulations of the flow [53,54].

Data accessibility. In compliance with EPSRC's open access initiative, the data in this paper is available from [67].

Declaration of AI use. We have not used AI-assisted technologies in creating this article.

Authors' contributions. R.E.: formal analysis, funding acquisition, investigation, methodology, visualization, writing—original draft, writing—review and editing; R.A.V.G.: formal analysis, investigation, methodology, visualization, writing—original draft, writing—review and editing.

Both authors gave final approval for publication and agreed to be held accountable for the work performed therein.

Conflict of interest declaration. We declare we have no competing interests.

Funding. This work was supported by the Engineering and Physical Sciences Research Council, grant number EP/V047469/1, awarded to RE.

Acknowledgements. RVG was a Visiting Scholar at Merton College and the Mathematical Institute, University of Oxford, UK, and a CNRS sponsored INP Guest Scientist at the Institut de Physique de Nice, France in the first half of 2023 while parts of this paper were completed, and thanks these organizations for their hospitality and support over this time.

References

1. Einstein A. 1905 On the motion of small particles suspended in liquids at rest required by the molecular-kinetic theory of heat. *Ann. Phys.* **17**, 208.
2. Chandrasekhar S. 1943 Stochastic problems in physics and astronomy. *Rev. Mod. Phys.* **15**, 1–89. (doi:10.1103/RevModPhys.15.1)

3. Mazur P, Oppenheim I. 1970 Molecular theory of Brownian motion. *Phys.* **50**, 241–258. (doi:10.1016/0031-8914(70)90005-4)
4. Langevin P. 1908 Sur la théorie du mouvement brownien. *Compt. Rendus* **146**, 530
5. Holley R. 1971 The motion of a heavy particle in an infinite one dimensional gas of hard spheres. *Z. Wahrsch. verw. Geb.* **17**, 181–219. (doi:10.1007/BF00536757)
6. Dürr D, Goldstein S, Lebowitz JL. 1981 A mechanical model of Brownian motion. *Commun. Math. Phys.* **78**, 507–530. (doi:10.1007/BF02046762)
7. Erban R, Chapman SJ. 2020 *Stochastic modelling of reaction-diffusion processes*. Cambridge, UK: Cambridge University Press. (doi:10.1017/9781108628389)
8. Erban R. 2014 From molecular dynamics to Brownian dynamics. *Proc. R. Soc. A* **470**, 20140036. (doi:10.1098/rspa.2014.0036)
9. Gunaratne RS, Wilson DB, Flegg MB, Erban R. 2019 Multi-resolution dimer models in heat baths with short-range and long-range interactions. *Interface Focus* **9**, 20180070. (doi:10.1098/rsfs.2018.0070)
10. Dunkel J, Hänggi P. 2006 Relativistic Brownian motion: from a microscopic binary collision model to the Langevin equation. *Phys. Rev. E* **74**, 051106. (doi:10.1103/PhysRevE.74.051106)
11. Wulfert R, Oechsle M, Speck T, Seifert U. 2017 Driven Brownian particle as a paradigm for a nonequilibrium heat bath: effective temperature and cyclic work extraction. *Phys. Rev. E* **95**, 050103. (doi:10.1103/PhysRevE.95.050103)
12. Goswami K. 2019 Work fluctuation relations for a dragged Brownian particle in active bath. *Physica A* **525**, 223–233. (doi:10.1016/j.physa.2019.03.050)
13. Nicolis G. 1965 On the evaluation of the thermal-diffusion coefficient of heavy particles using a theory of Brownian motion in a nonuniform medium. *J. Chem. Phys.* **43**, 1110–1112. (doi:10.1063/1.1696890)
14. Pérez-Madrid A, Rubí JM, Mazur P. 1994 Brownian motion in the presence of a temperature gradient. *Physica A* **212**, 231–238. (doi:10.1016/0378-4371(94)90329-8)
15. Pal PS, Rana S, Saha A, Jayannavar AM. 2014 Extracting work from a single heat bath: a case study of a Brownian particle under an external magnetic field in the presence of information. *Phys. Rev. E* **90**, 022143. (doi:10.1103/PhysRevE.90.022143)
16. Tóthová J, Šoltýs A, Lisý V. 2020 Brownian motion in a bath responding to external electric fields. *J. Mol. Liq.* **317**, 113920. (doi:10.1016/j.molliq.2020.113920)
17. Saffman PG. 1976 Brownian motion in thin sheets of viscous fluid. *J. Fluid Mech.* **73**, 593–602. (doi:10.1017/S0022112076001511)
18. Batchelor GK. 1977 The effect of Brownian motion on the bulk stress in a suspension of spherical particles. *J. Fluid Mech.* **83**, 97–117. (doi:10.1017/S0022112077001062)
19. Ramshaw JD. 1979 Brownian motion in a flowing fluid. *The Phys. of Fluids* **22**, 1595–1601. (doi:10.1063/1.862818)
20. Russel WB. 1981 Brownian motion of small particles suspended in liquids. *Annu. Rev. Fluid Mech.* **13**, 425–455. (doi:10.1146/annurev.fl.13.010181.002233)
21. Miyazaki K, Bedeaux D. 1995 Brownian motion in a fluid in simple shear flow. *Physica A* **217**, 53–74. (doi:10.1016/0378-4371(95)00077-K)
22. Hauge EH, Martin-Löf A. 1973 Fluctuating hydrodynamics and Brownian motion. *J. Stat. Phys.* **7**, 259–281. (doi:10.1007/BF01030307)
23. Bian X, Kim C, Karniadakis GE. 2016 111 years of Brownian motion. *Soft Matter* **12**, 6331–6346. (doi:10.1039/c6sm01153e)
24. Stokes G. 1851 On the effect of the internal friction of fluids on the motion of pendulums. *Trans. Camb. Philos. Soc.* **9**, 8.
25. Ho BP, Leal LG. 1974 Inertial migration of rigid spheres in two-dimensional unidirectional flows. *J. Fluid Mech.* **65**, 365–400. (doi:10.1017/S0022112074001431)
26. Maxey MR, Riley JJ. 1983 Equation of motion for a small rigid sphere in a nonuniform flow. *The Phys. of Fluids* **26**, 883–889. (doi:10.1063/1.864230)
27. Feng J, Hu HH, Joseph DD. 1994 Direct simulation of initial value problems for the motion of solid bodies in a Newtonian fluid. *J. Fluid Mech.* **277**, 271–301. (doi:10.1017/S0022112094002764)
28. Viecelli JA. 1993 Statistical mechanics and correlation properties of a rotating two-dimensional flow of like-sign vortices. *Phys. Fluids A* **5**, 2484–2501. (doi:10.1063/1.858762)

29. Solomon T, Weeks ER, Swinney HL. 1993 Observation of anomalous diffusion and Lévy flights in a two-dimensional rotating flow. *Phys. Rev. Lett.* **71**, 3975–3978. (doi:10.1103/PhysRevLett.71.3975)
30. Klafter J, Shlesinger MF, Zumofen G. 1996 Beyond Brownian motion. *Phys. Today* **49**, 33–39. (doi:10.1063/1.881487)
31. Gallagher I. 2019 From Newton to Navier-Stokes, or how to connect fluid mechanics equations from microscopic to macroscopic scales. *Bull. New Ser. Am. Math. Soc.* **56**, 65–85. (doi:10.1090/bull/1650)
32. Li T, Kheifets S, Medellin D, Raizen MG. 2010 Measurement of the instantaneous velocity of a Brownian particle. *Science* **328**, 1673–1675. (doi:10.1126/science.1189403)
33. Rubi JM, Bedeaux D. 1988 Brownian motion in a fluid in elongational flow. *J. Stat. Phys.* **53**, 125–136. (doi:10.1007/BF01011549)
34. Gotoh T. 1990 Brownian motion in a rotating flow. *J. Stat. Phys.* **59**, 371–402. (doi:10.1007/BF01015575)
35. Katayama Y, Terauti R. 1996 Brownian motion of a single particle under shear flow. *Eur. J. Phys.* **17**, 136–140. (doi:10.1088/0143-0807/17/3/007)
36. Garbaczewski P. 1998 Diffusion process in a flow. *Phys. Rev. E* **57**, 569–573. (doi:10.1103/PhysRevE.57.569)
37. Orihara H, Takikawa Y. 2011 Brownian motion in shear flow: direct observation of anomalous diffusion. *Phys. Rev. E* **84**, 061120. (doi:10.1103/PhysRevE.84.061120)
38. Wang N, Dagan Y. 2022 A generalized theory of Brownian particle diffusion in shear flows. *arXiv Preprint arXiv (doi: 10.48550/arXiv.2211.03825)*
39. Dobson M, Legoll F, Lelièvre T, Stoltz G. 2013 Derivation of Langevin dynamics in a nonzero background flow field. *ESAIM: M2AN* **47**, 1583–1626. (doi:10.1051/m2an/2013077)
40. Foister RT, Ven TGMVD. 1980 Diffusion of Brownian particles in shear flows. *J. Fluid Mech.* **96**, 105. (doi:10.1017/S0022112080002042)
41. Kusuoka S, Liang S. 2010 A classical mechanical model of Brownian motion with plural particles. *Rev. Math. Phys.* **22**, 733–838. (doi:10.1142/S0129055X10004077)
42. Kim C, Karniadakis GE. 2013 Microscopic theory of Brownian motion revisited: the Rayleigh model. *Phys. Rev. E* **87**, 032129. (doi:10.1103/PhysRevE.87.032129)
43. Rouyer F, Menon N. 2000 Velocity fluctuations in a homogeneous 2D granular gas in steady state. *Phys. Rev. Lett.* **85**, 3676–3679. (doi:10.1103/PhysRevLett.85.3676)
44. Aranson IS, Olafsen JS. 2002 Velocity fluctuations in electrostatically driven granular media. *Phys. Rev. E* **66**, 061302. (doi:10.1103/PhysRevE.66.061302)
45. van Noije TPC, Ernst MH. 1998 Velocity distributions in homogeneous granular fluids: the free and the heated case. *Granul. Matter* **1**, 57–64. (doi:10.1007/s100350050009)
46. Kohlstedt K, Snezhko A, Sapozhnikov MV, Aranson IS, Olafsen JS, Ben-Naim E. 2005 Velocity distributions of granular gases with drag and with long-range interactions. *Phys. Rev. Lett.* **95**, 068001. (doi:10.1103/PhysRevLett.95.068001)
47. Cairns RA, Mamum AA, Bingham R, Boström R, Dendy RO, Nairn CMC, Shukla PK. 1995 Electrostatic solitary structures in non-thermal plasmas. *Geophys. Res. Lett.* **22**, 2709–2712. (doi:10.1029/95GL02781)
48. Izacard O. 2017 Generalized fluid theory including non-Maxwellian kinetic effects. *J. Plasma Phys.* **83**, 595830201. (doi:10.1017/S0022377817000150)
49. Mo J, Raizen MG. 2019 Highly resolved Brownian motion in space and in time. *Annu. Rev. Fluid Mech.* **51**, 403–428. (doi:10.1146/annurev-fluid-010518-040527)
50. Erban R. 2016 Coupling all-atom molecular dynamics simulations of ions in water with Brownian dynamics. *Proc. R. Soc. A* **472**, 20150556. (doi:10.1098/rspa.2015.0556)
51. Erban R, Togashi Y. 2023 Asymmetric periodic boundary conditions for all-atom molecular dynamics and coarse-grained simulations of nucleic acids. *J. Phys. Chem. B* **127**, 8257–8267. (doi:10.1021/acs.jpcb.3c03887)
52. Shin HK, Kim C, Talkner P, Lee EK. 2010 Brownian motion from molecular dynamics. *Chem. Phys.* **375**, 316–326. (doi:10.1016/j.chemphys.2010.05.019)
53. Erban R. 2020 Coarse-graining molecular dynamics: stochastic models with non-Gaussian force distributions. *J. Math. Biol.* **80**, 457–479. (doi:10.1007/s00285-019-01433-5)
54. Utterson J, Erban R. 2022 On standardised moments of force distribution in simple liquids. *Phys. Chem. Chem. Phys.* **24**, 5646–5657. (doi:10.1039/d1cp04056a)

55. Cohen EGD. 1993 Fifty years of kinetic theory. *Physica A* **194**, 229–257. (doi:10.1016/0378-4371(93)90357-A)
56. Izacard O. 2016 Kinetic corrections from analytic non-Maxwellian distribution functions in magnetized plasmas. *Phys. Plasmas* **23**, 082504. (doi:10.1063/1.4960123)
57. Batchelor GK. 1967 *An introduction to fluid dynamics*. Cambridge, UK: Cambridge University Press.
58. Landau LD, Lifshitz EM. 1987 *Fluid mechanics: landau and lifshitz: course of theoretical physics*. vol. **6**. Oxford, UK: Pergamon Press.
59. Taylor GI. 1934 The formation of emulsions in definable fields of flow. *Proc. R. Soc. Lond. A* **146**, 501–523. (doi:10.1098/rspa.1934.0169)
60. Moffatt HK, Kida S, Ohkitani K. 1994 Stretched vortices - the sinews of turbulence; large-Reynolds-number asymptotics. *J. Fluid Mech.* **259**, 241–264. (doi:10.1017/S002211209400011X)
61. Sutera SP, Skalak R. 1993 The history of Poiseuille's law. *Annu. Rev. Fluid Mech.* **25**, 1–20. (doi:10.1146/annurev.fl.25.010193.000245)
62. Crane LJ. 1970 Flow past a stretching plate. *J. Appl. Math. Phys. (ZAMP)* **21**, 645–647. (doi:10.1007/BF01587695)
63. Robert CP. 1995 Simulation of truncated normal variables. *Stat. Comput.* **5**, 121–125. (doi:10.1007/BF00143942)
64. Franz B, Taylor-King JP, Yates C, Erban R. 2016 Hard-sphere interactions in velocity-jump models. *Phys. Rev. E* **94**, 012129. (doi:10.1103/PhysRevE.94.012129)
65. Ermak DL, McCammon JA. 1978 Brownian dynamics with hydrodynamic interactions. *J. Chem. Phys.* **69**, 1352–1360. (doi:10.1063/1.436761)
66. Rolls E, Erban R. 2018 Multi-resolution polymer Brownian dynamics with hydrodynamic interactions. *J. Chem. Phys.* **148**, 194111. (doi:10.1063/1.5018595)
67. Erban R. 2024 Supporting data for the paper "Langevin dynamics for a heavy particle immersed within a flow of light particles". University of Oxford. See https://ora.ox.ac.uk/objects/uuid:43401ead-ff2d-42e0-b4e5-a8a09385c2db.